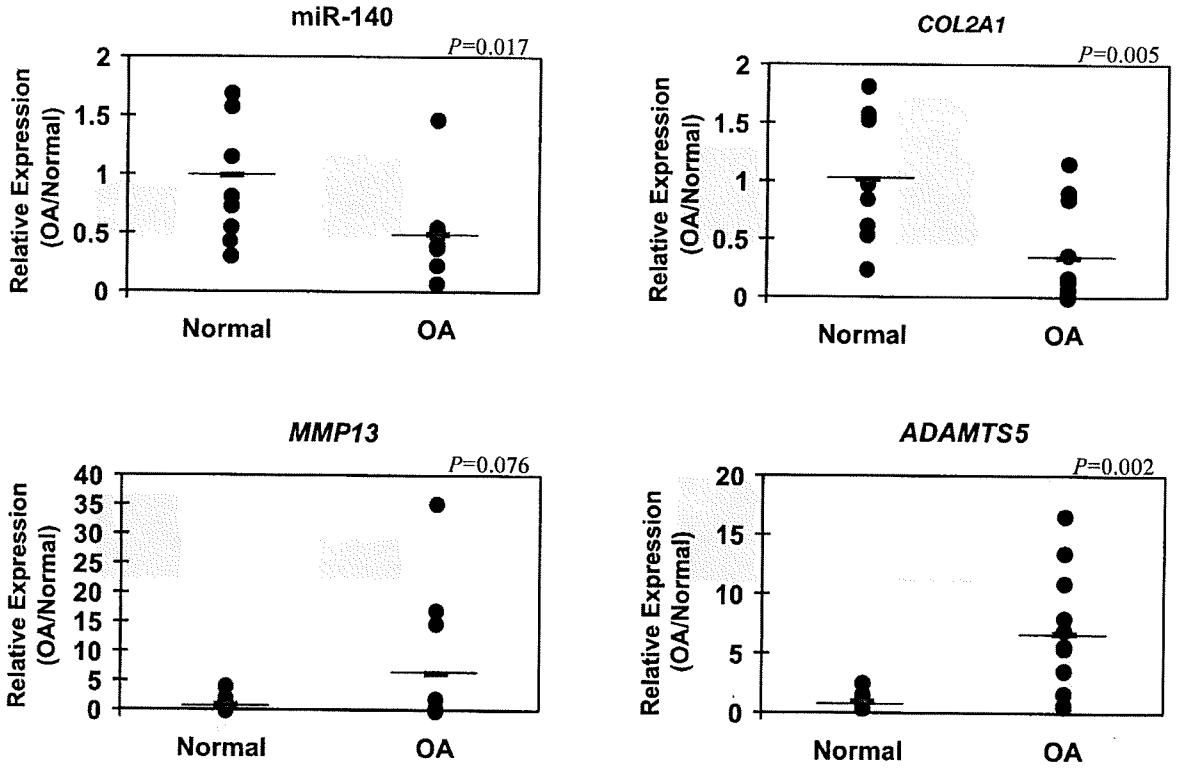

Figure 3. MicroRNA-140 (miR-140) expression in normal and osteoarthritis (OA) articular cartilage. Full-thickness cartilage specimens were collected from normal (n = 8) and OA (n = 11) knee joints for RNA isolation. The expression of miR-140, *COL2A1*, *ADAMTS5*, and *SOX9* was determined by quantitative polymerase chain reaction. The expression of miR-140 and *COL2A1* was significantly decreased, and the expression of *ADAMTS5* was significantly increased in OA cartilage compared with normal cartilage. Bars show the mean.

AGGRECAN (Hs00202971_m1), *ADAMTS5* (Hs00199841_m1), *MMP13* (Hs00233992_m1), and *GAPDH* (Hs99999905_m1) (Applied Biosystems). The U18 and GAPDH genes were used as an internal control to normalize differences in each sample. The expression levels for each gene were assessed relative to the expression of U18 or GAPDH.

Statistical analysis. Statistically significant differences between 2 groups were determined with *t*-tests. The results are reported as the mean ± SEM. *P* values less than 0.05 were considered significant.

RESULTS

MicroRNA-140 expression in articular chondrocytes and MSCs. Chondrogenic differentiation of MSCs involves dynamic changes in various gene expression patterns such as induced expression of chondrocyte-specific genes, including *SOX9* and *COL2A1*. In order to screen miRNA specifically expressed in chondrocytes, we performed gene expression profiling using miRNA microarrays comparing primary chondrocytes from articular cartilage with MSCs. Several miRNA were more abundant in primary articular chondrocytes than in undifferentiated MSCs. The largest difference was observed for miR-140 (Table 1). The high expression of miR-140 in chondrocytes compared with MSCs was confirmed by quantitative PCR (Figure 1).

Expression of miR-140 during chondrogenesis of MSCs. To examine the dynamic expression pattern of miR-140 during in vitro chondrogenesis, we performed a TaqMan quantitative PCR assay to analyze expression patterns of miR-140. Pellets of MSCs were strongly stained by Safranin O after chondrogenesis induction for 14 days (data not shown). In this model, miR-140 expression gradually increased during chondrogenesis in parallel with expression of *SOX9*, *AGGRECAN*, and *COL2A1* (Figure 2). These data indicate that the expres-

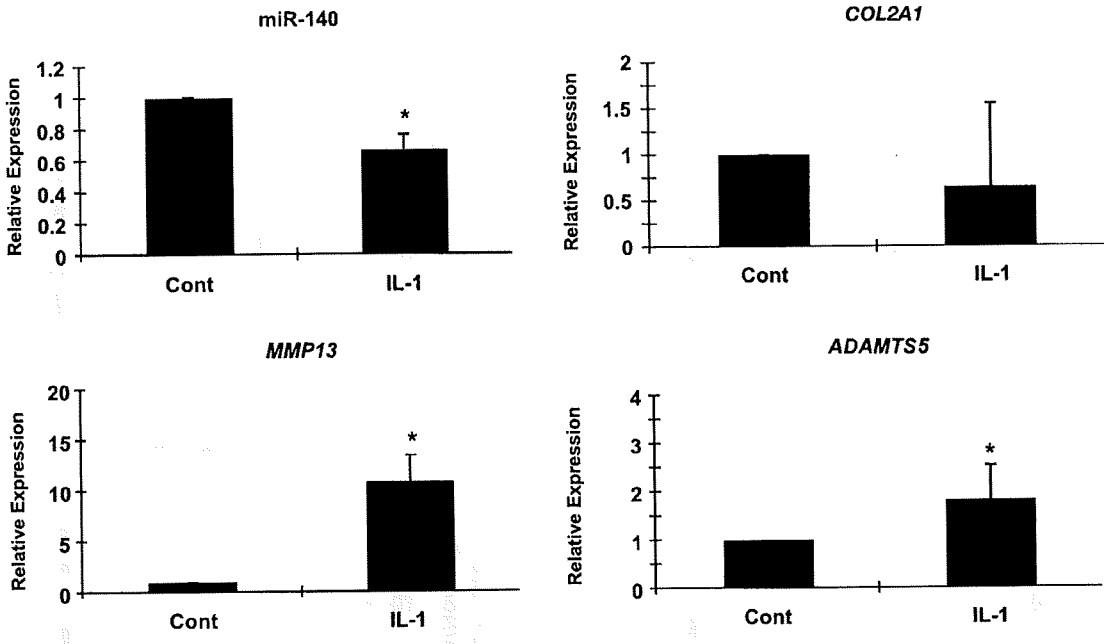

Figure 4. In vitro suppression of microRNA-140 (miR-140) by interleukin-1β (IL-1β). Articular chondrocytes (8 different preparations from 8 different donors) were treated with IL-1β (5 ng/ml) for 5 hours. The expression of miR-140, *COL2A1*, *MMP13*, and *ADAMTS5* was analyzed by quantitative polymerase chain reaction. IL-1β stimulation significantly decreased miR-140 expression and increased *MMP13* and *ADAMTS5* expression. *COL2A1* expression did not change significantly. Bars show the mean and SEM fold difference in relative expression. * = $P < 0.05$ versus control (Cont).

sion of miR-140 increases during chondrocytic differentiation of MSCs, and this is consistent with its high expression in chondrocytes.

Expression of miR-140 in normal and OA cartilage. In OA pathogenesis, several chondrocyte-specific genes, including *COL2A1* and *SOX9*, are down-regulated (23). In contrast, cartilage-degrading enzymes, including ADAMTS-5 and matrix metalloproteinase 13 (MMP-13), are up-regulated (24–26). To examine changes in miR-140 expression in OA articular cartilage, quantitative PCR of miR-140 together with OA-related marker genes was performed on 19 samples prepared from human knee articular cartilage (8 normal and 11 OA). As expected, the expression of *ADAMTS5* was significantly increased in OA cartilage, while the expression of *COL2A1* was significantly lower than that in normal cartilage (Figure 3). MiR-140 expression in articular cartilage from donors with OA (65–93 years old; Mankin score 5–10) was significantly lower than that in normal cartilage (obtained from individuals 30–44 years old; Mankin score 0–2) (Figure 3). These data demonstrate abnormally reduced miR-140 expression in OA cartilage and appear to correlate with increased *ADAMTS5* expression and reduced *COL2A1* expression in the same samples.

Effect of IL-1β on miR-140 expression in articular chondrocytes. IL-1β is one of the critical mediators of OA, and IL-1β stimulation of chondrocytes causes gene expression patterns similar to those of OA cartilage (27,28). To analyze the effects of IL-1β on the expression of miR-140 in articular chondrocytes, we performed quantitative PCR for miR-140 and *COL2A1*, *AGGRECAN*, *MMP13*, and *ADAMTS5*. In response to IL-1β stimulation, the expression of miR-140 was markedly decreased, while the expression of *MMP13* and *ADAMTS5* was significantly increased (Figure 4). Under the same experimental conditions, the expression of *COL2A1* did not change significantly. Taken together, these results show reduced miR-140 expression in the context of IL-1β–induced OA-like changes in chondrocyte gene expression.

Modulation of *ADAMTS5* and aggrecan expression in articular chondrocytes by miR-140. To investigate the function of miR-140 in chondrocytes, we examined whether expression of the OA-related genes *ADAMTS5*, *MMP13*, *COL2A1*, and *AGGRECAN* can be

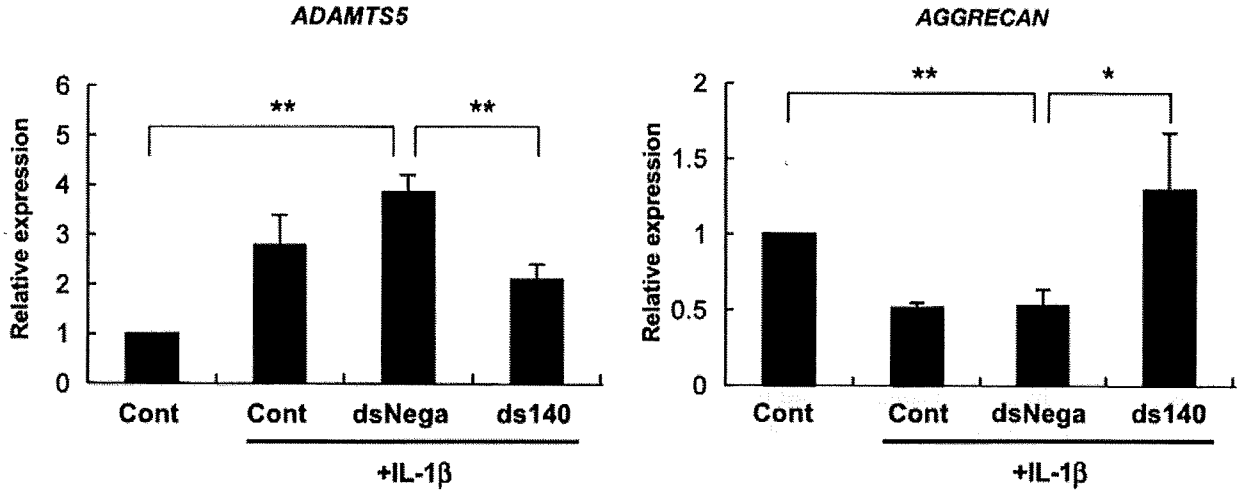

Figure 5. *ADAMTS5* and *AGGRECAN* expression by double-stranded microRNA-140 (ds–miR-140; ds140) in articular chondrocytes. Articular chondrocytes (n = 3) were transfected with ds–miR-140. The expression of *ADAMTS5* and *AGGRECAN* was analyzed by quantitative polymerase chain reaction. *ADAMTS5* expression was significantly reduced by ds–miR-140 with interleukin-1β (IL-1β) stimulation, and *AGGRECAN* expression was significantly increased by ds–miR-140 with IL-1β stimulation. Bars show the mean and SEM fold difference relative to control (Cont). dsNega = negative control of ds–miR-140 with nonspecific sequence. * = $P < 0.05$; ** = $P < 0.01$.

regulated by miR-140, when chondrocytes were stimulated with IL-1β with and without transfection of ds–miR-140. *ADAMTS5* expression with IL-1β stimulation was significantly reduced by ds–miR-140, and, conversely, *AGGRECAN* expression with IL-1β stimulation was significantly increased by ds–miR-140 (Figure 5). In the absence of IL-1β, the nonspecific dsRNA (dsNega) did not change the basal levels of *AGGRECAN*, and we observed an increase in *ADAMTS5* mRNA with ds–miR-140 as well as with dsNega. The expression of *MMP13* and *COL2A1* was not significantly changed by ds–miR-140 (data not shown). These results demonstrated that miR-140 regulates genes encoding ADAMTS-5 and aggrecan, suggesting that miR-140 plays an important role in regulating the balance between ECM formation and degradation.

DISCUSSION

This study is the first to identify miRNA that are expressed in a differentiation-dependent pattern in MSCs and articular chondrocytes. We also show changes in expression of the selected miR-140 in OA cartilage and in response to IL-1β stimulation. Moreover, we demonstrate that ADAMTS-5, a critical proteinase in OA pathogenesis (29–31), is regulated by miR-140.

Previous studies using systematic whole-mount in situ hybridization analysis for miRNA in zebrafish revealed that many miRNA are expressed in a tissue-specific pattern (32). From this database annotation, miR-140 was the only miRNA with a cartilage-specific expression pattern. Zebrafish embryos injected with ds–miR-140 had a profound facial phenotype, including cranial hemorrhaging and a hypoplastic roof of the mouth (33). Our miRNA array screen detected several miRNA that show large differences in expression in articular chondrocytes versus MSCs, including miR-140, which showed the largest expression difference between the 2 cell types. We also showed that during chondrogenesis, miR-140 expression increased in differentiated human MSCs compared with undifferentiated MSCs in parallel with expression of *SOX9*, *AGGRECAN*, and *COL2A1*. These findings suggest that miR-140 is a marker and possibly a regulator of chondrocyte differentiation.

The unique differentiation-related expression pattern of miR-140 is highlighted by our findings for miR-146, which is also expressed in chondrocytes. In contrast to miR-140, miR-146 has a broader tissue distribution, its expression is increased in response to IL-1 stimulation, it is up-regulated in OA (34), and it does not show changes related to chondrocyte differentiation (data not shown).

The ability of chondrocytes to remodel and repair cartilage ECM declines with aging, and in OA this is

related to a decline in the anabolic activity of chondrocytes (35,36). The expression of miR-140 was reduced in OA cartilage, and, in the same samples, expression of the proteinase *ADAMTS5* increased, and *COL2A1* expression decreased. Thus, the abnormal expression pattern of miR-140 correlates with the imbalance of anabolic–catabolic responses in OA. Our observations of abnormal miR-140 expression in OA are consistent with the findings of a recent study (37). IL-1β is one of the most prominent mediators of cartilage degradation and joint inflammation (38,39). IL-1β induces a cascade of inflammatory and catabolic events in chondrocytes. It also changes chondrocyte anabolism by suppressing the synthesis of proteoglycans and collagens and by enhancing the production of MMPs (27,28). The expression of miR-140 was down-regulated by IL-1β stimulation of chondrocytes in vitro. These data suggest that IL-1β may be a mediator that is involved in the suppression of miR-140 in OA.

Our studies using dsRNA mimicking miR-140 suggest that miR-140 suppresses *ADAMTS5* mRNA expression. This observation is supported by preliminary observations of increased *ADAMTS5* expression in miR-140–knockout mice (Miyaki S, et al: unpublished observations). The pathogenesis of OA is associated with abnormal activation and differentiation of chondrocytes that overexpress inflammation mediators and matrix-degrading enzymes (3–6). Previously examined mechanisms in these abnormal cellular responses include chondrocyte stimulation by extracellular stimuli such as cytokines, growth factors, mechanical stress, and matrix-degradation products. Intracellularly, these stimuli activate signaling cascades that lead to changes in gene expression (23,40). Alteration of miR-140 by IL-1β represents a novel mechanism to explain such aberrant changes in chondrocyte gene expression.

The present study was focused on miR-140, because it was shown to be the most cartilage-specific miRNA. We performed searches in 3 databases (TargetScan [http://www.targetscan.org/vert_50/], PicTar [http://pictar.mdc-berlin.de/], and miRanda [http://microrna.sanger.ac. uk/]), and this yielded 223–975 potential miR-140 targets. Only 9 potential targets were identified in all 3 databases, and, notably, this did not include *ADAMTS5*. Uncertainty remains regarding the rules for in silico miRNA target identification (41). At present, the most conclusive target validation is the demonstration of changes in protein expression, cell function, or phenotype in knockout or transgenic mice. Future studies are needed to determine the consequences of changes in the complete set of miR-140 targets for cartilage development and homeostasis. Currently, ongoing studies with miR-140–knockout mice and miR-140–transgenic mice will provide information in this regard.

In conclusion, the results of this study suggest that miR-140 is a chondrocyte differentiation–related miRNA. It may be a novel regulator of cartilage homeostasis, and changes in its expression and function play an important role in diseases affecting articular cartilage. Further studies of miR-140 have the potential to reveal important new regulatory pathways that control cartilage development and homeostasis and provide new insights into disease mechanisms and therapeutic interventions for OA.

AUTHOR CONTRIBUTIONS

All authors were involved in drafting the article or revising it critically for important intellectual content, and all authors approved the final version to be published. Dr. Asahara had full access to all of the data in the study and takes responsibility for the integrity of the data and the accuracy of the data analysis.

Study conception and design. Miyaki, Asahara.

Acquisition of data. Miyaki, Nakasa, Otsuki, Grogan, Higashiyama, Inoue.

Analysis and interpretation of data. Miyaki, Nakasa, Otsuki, Grogan, Inoue, Kato, Sato, Lotz.

REFERENCES

1. Lawrence RC, Felson DT, Helmick CG, Arnold LM, Choi H, Deyo RA, et al. Estimates of the prevalence of arthritis and other rheumatic conditions in the United States. Part II. Arthritis Rheum 2008;58:26–35.
2. Helmick CG, Felson DT, Lawrence RC, Gabriel S, Hirsch R, Kwoh CK, et al. Estimates of the prevalence of arthritis and other rheumatic conditions in the United States. Part I. Arthritis Rheum 2008;58:15–25.
3. Goldring MB. The role of the chondrocyte in osteoarthritis [review]. Arthritis Rheum 2000;43:1916–26.
4. Lotz M. Cytokines in cartilage injury and repair. Clin Orthop Relat Res 2001;(391 Suppl):S108–15.
5. Kuhn K, D'Lima DD, Hashimoto S, Lotz M. Cell death in cartilage. Osteoarthritis Cartilage 2004;12:1–16.
6. Goldring MB. Update on the biology of the chondrocyte and new approaches to treating cartilage diseases. Best Pract Res Clin Rheumatol 2006;20:1003–25.
7. Lagos-Quintana M, Rauhut R, Lendeckel W, Tuschl T. Identification of novel genes coding for small expressed RNAs. Science 2001;294:853–8.
8. Bartel DP. MicroRNAs: genomics, biogenesis, mechanism, and function. Cell 2004;116:281–97.
9. Lee RC, Ambros V. An extensive class of small RNAs in Caenorhabditis elegans. Science 2001;294:862–4.
10. Lau NC, Lim LP, Weinstein EG, Bartel DP. An abundant class of tiny RNAs with probable regulatory roles in Caenorhabditis elegans. Science 2001;294:858–62.
11. Lewis BP, Burge CB, Bartel DP. Conserved seed pairing, often flanked by adenosines, indicates that thousands of human genes are microRNA targets. Cell 2005;120:15–20.

12. Esquela-Kerscher A, Slack FJ. Oncomirs: microRNAs with a role in cancer. Nat Rev Cancer 2006;6:259–69.
13. Van Rooij E, Sutherland LB, Liu N, Williams AH, McAnally J, Gerard RD, et al. A signature pattern of stress-responsive microRNAs that can evoke cardiac hypertrophy and heart failure. Proc Natl Acad Sci U S A 2006;103:18255–60.
14. Poy MN, Eliasson L, Krutzfeldt J, Kuwajima S, Ma X, Macdonald PE, et al. A pancreatic islet-specific microRNA regulates insulin secretion. Nature 2004;432:226–30.
15. Nakasa T, Miyaki S, Okubo A, Hashimoto M, Nishida K, Ochi M, et al. Expression of microRNA-146 in rheumatoid arthritis synovial tissue. Arthritis Rheum 2008;58:1284–92.
16. Stanczyk J, Pedrioli DM, Brentano F, Sanchez-Pernaute O, Kolling C, Gay RE, et al. Altered expression of microRNA in synovial fibroblasts and synovial tissue in rheumatoid arthritis. Arthritis Rheum 2008;58:1001–9.
17. Harfe BD, McManus MT, Mansfield JH, Hornstein E, Tabin CJ. The RNaseIII enzyme Dicer is required for morphogenesis but not patterning of the vertebrate limb. Proc Natl Acad Sci U S A 2005;102:10898–903.
18. Kobayashi T, Lu J, Cobb BS, Rodda SJ, McMahon AP, Schipani E, et al. Dicer-dependent pathways regulate chondrocyte proliferation and differentiation. Proc Natl Acad Sci U S A 2008;105:1949–54.
19. Tuddenham L, Wheeler G, Ntounia-Fousara S, Waters J, Hajihosseini MK, Clark I, et al. The cartilage specific microRNA-140 targets histone deacetylase 4 in mouse cells. FEBS Lett 2006;580:4214–7.
20. Mankin HJ, Dorfman H, Lippiello L, Zarins A. Biochemical and metabolic abnormalities in articular cartilage from osteo-arthritic human hips. II. Correlation of morphology with biochemical and metabolic data. J Bone Joint Surg Am 1971;53:523–37.
21. Maier R, Ganu V, Lotz M. Interleukin-11, an inducible cytokine in human articular chondrocytes and synoviocytes, stimulates the production of the tissue inhibitor of metalloproteinases. J Biol Chem 1993;268:21527–32.
22. Grogan SP, Olee T, Hiraoka K, Lotz MK. Repression of chondrogenesis through binding of notch signaling proteins HES-1 and HEY-1 to N-box domains in the COL2A1 enhancer site. Arthritis Rheum 2008;58:2754–63.
23. Hashimoto M, Nakasa T, Hikata T, Asahara H. Molecular network of cartilage homeostasis and osteoarthritis. Med Res Rev 2008;28:464–81.
24. Mitchell PG, Magna HA, Reeves LM, Lopresti-Morrow LL, Yocum SA, Rosner PJ, et al. Cloning, expression, and type II collagenolytic activity of matrix metalloproteinase-13 from human osteoarthritic cartilage. J Clin Invest 1996;97:761–8.
25. Bau B, Gebhard PM, Haag J, Knorr T, Bartnik E, Aigner T. Relative messenger RNA expression profiling of collagenases and aggrecanases in human articular chondrocytes in vivo and in vitro. Arthritis Rheum 2002;46:2648–57.
26. Malfait AM, Liu RQ, Ijiri K, Komiya S, Tortorella MD. Inhibition of ADAM-TS4 and ADAM-TS5 prevents aggrecan degradation in osteoarthritic cartilage. J Biol Chem 2002;277:22201–8.
27. Goldring MB, Birkhead J, Sandell LJ, Kimura T, Krane SM. Interleukin 1 suppresses expression of cartilage-specific types II and IX collagens and increases types I and III collagens in human chondrocytes. J Clin Invest 1988;82:2026–37.
28. Lefebvre V, Peeters-Joris C, Vaes G. Modulation by interleukin 1 and tumor necrosis factor α of production of collagenase, tissue inhibitor of metalloproteinases and collagen types in differentiated and dedifferentiated articular chondrocytes. Biochim Biophys Acta 1990;1052:366–78.
29. Glasson SS, Askew R, Sheppard B, Carito B, Blanchet T, Ma HL, et al. Deletion of active ADAMTS5 prevents cartilage degradation in a murine model of osteoarthritis. Nature 2005;434:644–8.
30. Stanton H, Rogerson FM, East CJ, Golub SB, Lawlor KE, Meeker CT, et al. ADAMTS5 is the major aggrecanase in mouse cartilage in vivo and in vitro. Nature 2005;434:648–52.
31. Little CB, Meeker CT, Golub SB, Lawlor KE, Farmer PJ, Smith SM, et al. Blocking aggrecanase cleavage in the aggrecan interglobular domain abrogates cartilage erosion and promotes cartilage repair. J Clin Invest 2007;117:1627–36.
32. Wienholds E, Kloosterman WP, Miska E, Alvarez-Saavedra E, Berezikov E, de Bruijn E, et al. MicroRNA expression in zebrafish embryonic development. Science 2005;309:310–1.
33. Eberhart JK, He X, Swartz ME, Yan YL, Song H, Boling TC, et al. MicroRNA Mirn140 modulates Pdgf signaling during palatogenesis. Nat Genet 2008;40:290–8.
34. Yamasaki K, Nakasa T, Miyaki S, Ishikawa M, Deie M, Adachi N, et al. Expression of MicroRNA-146a in osteoarthritis cartilage. Arthritis Rheum 2009;60:1035–41.
35. Dudhia J. Aggrecan, aging and assembly in articular cartilage. Cell Mol Life Sci 2005;62:2241–56.
36. Aigner T, Soder S, Gebhard PM, McAlinden A, Haag J. Mechanisms of disease: role of chondrocytes in the pathogenesis of osteoarthritis: structure, chaos and senescence. Nat Clin Pract Rheumatol 2007;3:391–9.
37. Iliopoulos D, Malizos KN, Oikonomou P, Tsezou A. Integrative microRNA and proteomic approaches identify novel osteoarthritis genes and their collaborative metabolic and inflammatory networks. PLoS ONE 2008;3:e3740.
38. Goldring MB. Osteoarthritis and cartilage: the role of cytokines. Curr Rheumatol Rep 2000;2:459–65.
39. Zwerina J, Redlich K, Polzer K, Joosten L, Kronke G, Distler J, et al. TNF-induced structural joint damage is mediated by IL-1. Proc Natl Acad Sci U S A 2007;104:11742–7.
40. Goldring MB, Goldring SR. Osteoarthritis. J Cell Physiol 2007;213:626–34.
41. Kuhn DE, Martin MM, Feldman DS, Terry AV Jr, Nuovo GJ, Elton TS. Experimental validation of miRNA targets. Methods 2008;44:47–54.

The International Journal of Biochemistry & Cell Biology 41 (2009) 1198–1204

Contents lists available at ScienceDirect

The International Journal of Biochemistry & Cell Biology

journal homepage: www.elsevier.com/locate/biocel

Smad3 activates the Sox9-dependent transcription on chromatin

Takayuki Furumatsu[a,b,*], Toshifumi Ozaki[a], Hiroshi Asahara[b,c,**]

[a] Department of Orthopaedic Surgery, Okayama University Graduate School, 2-5-1 Shikatacho, Okayama 700-8558, Japan
[b] Department of Molecular and Experimental Medicine, The Scripps Research Institute, 10550 North Torrey Pines Road, La Jolla, CA 92037, USA
[c] National Center for Child Health and Development, 2-10-1 Okura, Setagaya, Tokyo 157-8535, Japan

ARTICLE INFO

Article history:
Received 1 August 2008
Received in revised form 19 October 2008
Accepted 29 October 2008
Available online 8 November 2008

Keywords:
Chondrogenesis
Chromatin
p300
Smad3
Sox9

ABSTRACT

Transforming growth factor (TGF)-β has an essential role for the Sry-type high-mobility-group box (Sox)-regulated chondrogenesis. Chondrogenic differentiation is also controlled by chromatin-mediated transcription. We have previously reported that TGF-β-regulated Smad3 induces chondrogenesis through the activation of Sox9-dependent transcription. However, the cross-talk between TGF-β signal and Sox9 on chromatin-mediated transcription has not been elucidated. In the present study, we investigated the activity of Smad3, Sox9, and coactivator p300 using an in vitro chromatin assembly model. Luciferase reporter assays revealed that Smad3 stimulated the Sox9-mediated transcription in a TGF-β-dependent manner. Recombinant Sox9 associated with phosphorylated Smad3/4 and recognized the enhancer region of type II collagen gene. In vitro transcription and S1 nuclease assays showed that Smad3 and p300 cooperatively activated the Sox9-dependent transcription on chromatin template. The combination treatment of phosphorylated Smad3, Sox9, and p300 were necessary for the activation of chromatin-mediated transcription. These findings suggest that TGF-β signal Smad3 plays a key role for chromatin remodeling to induce chondrogenesis via its association with Sox9.

1. Introduction

Chondrogenesis is the fundamental process to form bones and articular surfaces. Mesenchymal condensation and the following chondrocyte differentiation are strictly regulated by several transcription factors and growth factors, such as Sry-type high-mobility-group box (Sox) genes and the transforming growth factor (TGF)-β superfamily, respectively. Sox5, 6, and 9 cooperatively regulate the sequential differentiation steps of chondrogenesis (Akiyama et al., 2002, 2004; Stricker et al., 2002). In these transcription factors, Sox9 has an essential role to initiate mesenchymal condensation and to maintain chondrogenic potential in early stages. The expression of α1 chain of type II collagen (Col2a1), a major component of cartilage extracellular matrix, is controlled by Sox9 through the Sox9-binding site on the Col2a1 enhancer region (Bell et al., 1997) and closely parallels that of Sox9 (Ng et al., 1997). The TGF-β superfamily including the two major families (TGF-β and bone morphogenetic protein) is a multifunctional growth factor for many cellular responses such as differentiation and proliferation (Heldin et al., 1997; Shi and Massagué, 2003). In chondrogenesis, TGF-β stimulation is necessary for primary chondrogenesis derived from mesenchymal stem cells (Pittenger et al., 1999). We previously described that TGF-β signal Smad3 promotes the early chondrogenesis through the activation of Sox9 (Furumatsu et al., 2005a). However, the precise mechanisms of Sox9 and TGF-β in the epigenetic regulation for initiating chondrogenesis are still unclear.

The epigenetic regulation is another dynamic system to control gene expression and other fundamental cellular processes, such as proliferation and differentiation (Li, 2002; Felsenfeld and Groudine, 2003; Jaenisch and Bird, 2003). Chromatin remodeling system including histone modification is the representative mechanism of epigenetics. The eukaryotic DNA and histones are packaged into chromatin as the nucleosome-repeated structure. Accesses of transcription factors and other regulators to DNA are highly restricted by chromatin structure. Many molecules have been revealed as important factors to form chromatin. Nucleosome assembly protein-1 (NAP-1) acts as a histone-shuttling protein (Ito

Abbreviations: AcCoA, acetyl-coenzyme A; ACF, ATP-utilizing chromatin assembly and remodeling factor; Col2a1, α1 chain of type II collagen; EMSA, electrophoretic mobility shift assay; MNase, micrococcal nuclease; MAPK, mitogen-activated protein kinase; NAP-1, nucleosome assembly protein-1; si-, small interfering; Sox, Sry-type high-mobility-group box; TβR-I(TD), constitutively active form of TβR-I; TGF, transforming growth factor.

* Corresponding author at: Department of Orthopaedic Surgery, Okayama University Graduate School, 2-5-1 Shikatacho, Okayama 700-8558, Japan.
Tel.: +81 86 235 7273; fax: +81 86 223 9727.
** Corresponding author at: Department of Molecular and Experimental Medicine, The Scripps Research Institute, 10550 North Torrey Pines Road, La Jolla, CA 92037, USA.
E-mail addresses: matino@md.okayama-u.ac.jp (T. Furumatsu), asahara@scripps.edu (H. Asahara).

1357-2725/$ – see front matter © 2008 Elsevier Ltd. All rights reserved.
doi:10.1016/j.biocel.2008.10.032

et al., 1996; Nakagawa et al., 2001). ACF (ATP-utilizing chromatin assembly and remodeling factor), consisting of Acf1 and ISWI subunits, assembles periodic nucleosome arrays on histone-attached DNA in an ATP-dependent process (Ito et al., 1999; Nakagawa et al., 2001). On the other hand, histone modification on chromatin, such as acetylation, enables transcription regulators to access to DNA sequences. DNA-binding transcription factors, such as CREB and MyoD, exert their transcriptional potential on histone-acetylated chromatin (Asahara et al., 2001; Dilworth et al., 2004). However, the relationship between chromatin-mediated transcription and signaling molecules is not elucidated. We previously reported that p300, which has an intrinsic histone acetyltransferase activity, directly associates with Sox9 (Tsuda et al., 2003) and activates the Sox9-dependent transcription on chromatin (Furumatsu et al., 2005b). In this study, we further analyzed the cross-talk between the Sox9-dependent transcription and TGF-β receptor-regulated Smad3 on chromatin using an in vitro chromatin assembly model.

The present study demonstrates that TGF-β-stimulated Smad3 activates the Sox9-dependent transcription on chromatin. This is the first report to explain the importance of TGF-β treatment in chromatin-mediated chondrogenesis.

2. Materials and methods

2.1. Cells, plasmids, si-RNA, and antibodies

A human chondrosarcoma cell line (SW1353) was used as an immature chondrogenic cell line. A plasmid encoding full-length of rat Sox9 and a small interfering (si-) RNA against Smad3 were used (Furumatsu et al., 2005a). p300 was a gift from Tso-Pang Yao. FLAG-tagged Smad3/4 and the constitutively active form of TβR-I [TβR-I(TD)] were generous gifts from Takeshi Imamura. pGL3-585E, which contains a mouse Col2a1 promoter and enhancer, was constructed with a pGL3-Basic (Promega) vector and used as a native Col2a1 reporter gene. 12 × 48-pGL3-P containing 12 sets of a 48-bp Col2a1 enhancer element was used as a reporter plasmid. PCR fragments of FLAG-tagged Sox9, FLAG-tagged Smad3, and Smad4 were subcloned into baculovirus expression vector pENTR3C (Invitrogen) as described (Furumatsu et al., 2005b). The following antibodies were used: FLAG M2, FLAG M2 affinity gel (Sigma), phospho-Smad2/3 (Santa Cruz), Smad2/3 (Upstate), Smad4 (Cell Signaling), and Sox9 (Chemicon).

2.2. Luciferase reporter assay

pGL3-585E and 12 × 48-pGL3-P were used as reporter genes for investigating the Sox9-dependent transcriptional activity. These reporter plasmids were different from our previous constructs (Furumatsu et al., 2005a). Appropriate plasmids (50 ng) and si-Smad3 (200 nM) were transiently transfected into SW1353 cells using FuGENE6 (Roche). pRL-CMV (10 ng, Promega) was used as an internal control. The cells were harvested for 24 h, and then the luciferase activities were analyzed using Dual-Luciferase Reporter Assay System (Promega). The assays were performed in triplicate.

2.3. Nuclear extract and immunoprecipitation

Nuclear extracts of SW1353 cells were prepared in 2× buffer D [20 mM HEPES (pH 7.9), 20% glycerol, 0.1 M KCl, 0.2 mM EDTA, 0.5 mM PMSF, 0.5 mM DTT]. Protein concentrations were measured by BCA protein assay kit (Bio-Rad). Immunoprecipitation analyses using purified recombinant proteins were performed with anti-Sox9 or Smad2/3 antibody in 1× buffer D as described previously (Furumatsu et al., 2005b). Briefly, indicated amounts of recombinant proteins and/or nuclear extracts were incubated for 1 h at 25 °C. Ten percent volume of reaction mixture was loaded as an input fraction. Half of the mixture was incubated with each antibody and protein A beads (Sigma) for 1 h at 4 °C. Remaining mixture was incubated with rabbit IgG as a control.

2.4. Purification of histones and recombinant proteins

Core histones were purified from HeLa nuclear pellets and dialyzed in HEG buffer [10 mM HEPES (pH 7.6) 10% glycerol, 50 mM KCl, 0.1 mM EDTA]. Baculovirus of histidine-tagged NAP-1, FLAG-tagged ISWI, and Acf-1 were kindly gifts from Takashi Ito and used as chromatin assembling molecules (Ito et al., 1999, 2000). The baculovirus expression vectors carrying Sox9 and Smad3/4 were constructed using BaculoDirect Systems according to the manufacturer's protocol (Invitrogen). Recombinant NAP-1, recombinant ACF complex (FLAG-tagged ISWI and untagged Acf-1), FLAG-tagged p300, FLAG-tagged Sox9, and Smad3/4 complex (FLAG-tagged Smad3 and untagged Smad4) were produced in Sf9 cells (Invitrogen) and prepared as described previously (Furumatsu et al., 2005b). Recombinant Smad3/4 was purified after 30-min-treatments of TGF-β3 (R&D). Purified proteins were assessed by silver stain (BioRad) and Western blotting analyses.

2.5. Electrophoretic mobility shift assay (EMSA)

The Col2a1 enhancer probe containing the Sox9-binding site (in capital letters) was generated by annealing the following oligonucleotides: 5′-gcgcttgagaaaagcccCATTCATgagaggc-3′ and 5′-gcctctcATGAATGgggcttttctcaagcgc-3′. Probes were ^{32}P end-labeled using T4 polynucleotide kinase (Invitrogen). Purified Sox9 (30 ng) was incubated with the labeled probe (0.8 pmol). The unlabeled Col2a1 enhancer probe (16 pmol) was used as a competitor. In supershift analysis, 15 min treatment with anti-Sox9 antibody (0.2 μg) was performed before protein–DNA binding reaction.

2.6. Chromatin assembly and micrococcal nuclease (MNase) assay

Chromatin assembly and MNase digestion analyses were performed as described (Asahara et al., 2002) by using 12 × 48-pGL3-P. For chromatin reconstitution, standard reactions (20 μl) containing plasmid (150 ng), histones (100 ng), NAP-1 (500 ng), ISWI/Acf-1 (0.65 ng each), ATP (3 mM), and ATP regeneration systems (30 mM phosphocreatine and 20 ng creatine phosphokinase) were incubated at 30 °C for 4 h. In MNase assay, chromatinized plasmids (300 ng) were digested with MNase (0, 0.02, and 0.04 U/15 μl) for 5 min at 37 °C.

2.7. In vitro transcription and S1 nuclease assay

After chromatin assembly, standard reactions (12 × 48-pGL3-P, 150 ng) were incubated with Sox9 (10 ng), Smad3/4 (100 ng), p300 (40 ng), and acetyl-coenzyme A (AcCoA, 5 μM) for 30 min at 30 °C. For in vitro transcription, nuclear extracts from SW1353 cells (30 μg) were added and incubated with rNTPs at 30 °C for 40 min. In vitro-transcribed RNAs were recovered and subjected to S1 nuclease analyses using the specific primer (49 bp) against 12 × 48-pGL3-P luciferase gene as described (Furumatsu et al., 2005b). RNAs were annealed with ^{32}P end-labeled primers (0.2 pmol each) for 12 h, and then digested with 50 units of S1 nuclease (Invitrogen) for 30 min at 37 °C. The protected fragments were run on 8% denaturing polyacrylamide gels and visualized by autoradiography. Each experiment was performed at least three times.

3. Results

3.1. Smad3 stimulates the Sox9-mediated transcription in a TGF-β-dependent manner

To assess the fundamental role of Smad3 in chromatin remodeling during early chondrogenesis, we first analyzed the effect of Smad3 in the Sox9-regulated transcription using newly constructed reporter plasmids. Overexpressed Smad3 stimulated the transcriptional activity of Col2a1 reporter gene (Fig. 1A, pGL3-585E) in a Sox9-depedent manner (Fig. 1B). In addition, the effect of Smad3 was enhanced by the cotransfection of constitutively active form of TGF-β receptor I [TβR-I(TD)]. Twelve copies of the Sox9-binding fragment dramatically induced the Sox9-regulated transcription in reporter assays (Fig. 1C, 12 × 48-pGL3-P). Smad3 also activated the transcription of 12 × 48-pGL3-P in Sox9- and TGF-β-dependent manners. These findings suggest that Smad3 may act as a chromatin remodeling factor in chondrogenesis.

3.2. TGF-β and Smad3 are necessary for the activation of Sox9-dependent transcription

To investigate the effect of Smad3 itself in this reporter assay system, we used a si-RNA fragment against Smad3 as an inhibitor. The activities of Sox9-regulated transcription were stimulated by the addition of Smad3 in a dose-dependent fashion (Fig. 2A and B). si-Smad3 decreased the effect of activated TGF-β receptor and overexpressed Smad3 in Sox9-regulated reporters to the basal levels. However, si-Smad3 did not inhibit the Sox9-induced transactivation. These results prompted us to analyze the function of TGF-β-stimulated Smad3 and Sox9-related transcriptional apparatus on chromatin in chondrogenesis.

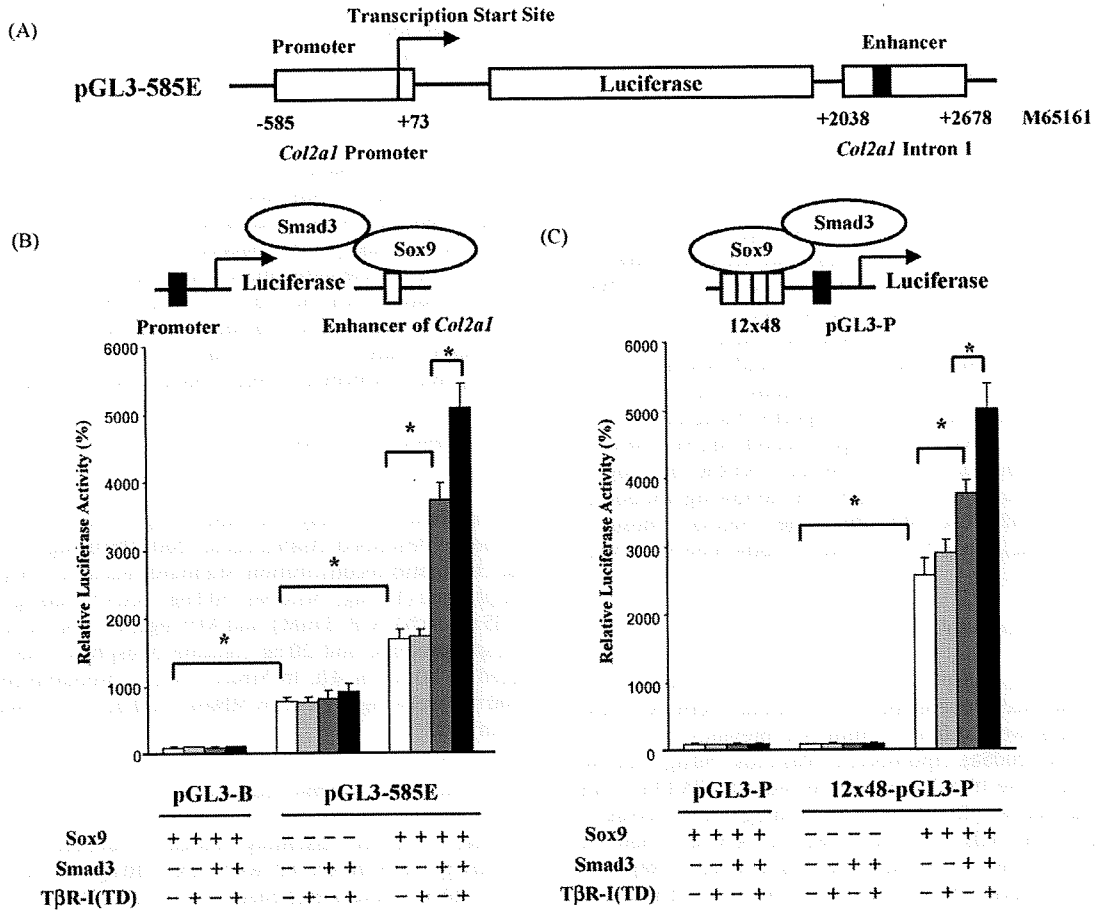

Fig. 1. Smad3 enhances the Sox9-mediated transcription in a TGF-β-dependent manner. (A) A schematic characterization of pGL3-585E which contains a native promoter and enhancer of mouse Col2a1 gene. Numbers indicate the distance from the transcription start site on mouse Col2a1 gene (National Center for Biotechnology Information, M65161). Black box denotes the SOX9-binding site on the enhancer region of Col2a1 intron 1. (B) Transient transfections of Sox9, Smad3, and TβR-I(TD) did not increase luciferase activities of pGL3-B plasmids in SW1353 cells (pGL3-B). In pGL3-585E systems, Sox9 enhanced a relative luciferase activity to a level as high as 2.2-fold over the control. Cotransfection of Smad3 augmented a luciferase activity up to 2.3-fold higher level of Sox9-transfected cells. The additional transfection of constitutively active form of TβR-I(TD) induced an approximately 36% increase of the activity in Sox9- and Smad3-transfected SW1353 cells. Luciferase activities of pGL3-585E were not increased in the absence of Sox9. Note that Smad3 and TβR-I(TD) synergistically activated the native Col2a1 reporter-mediated transcription in a Sox9-dependent manner. (C) The activity of 12 × 48 pGL3-P was enhanced by the addition of Sox9 up to 27.5-fold levels of the control. Smad3 increased the 12 × 48 pGL3-P-based luciferase activity up to 1.5-fold higher level in the presence of Sox9. TβR-I(TD) also induced 33% increase of the activity of Smad3-transfected cells in the presence of Sox9. However, the additional increase of luciferase activity was not observed in pGL3-P-transfected cells. Relative luciferase activities were calculated using the activity of pGL3-P as a control (100%). A schematic illustration of each reporter assay system is placed on the top of each figure (B and C). *Statistical significances ($p < 0.05$) were observed between the indicated bars with the Mann–Whitney *U*-test. Error bars, S.D.

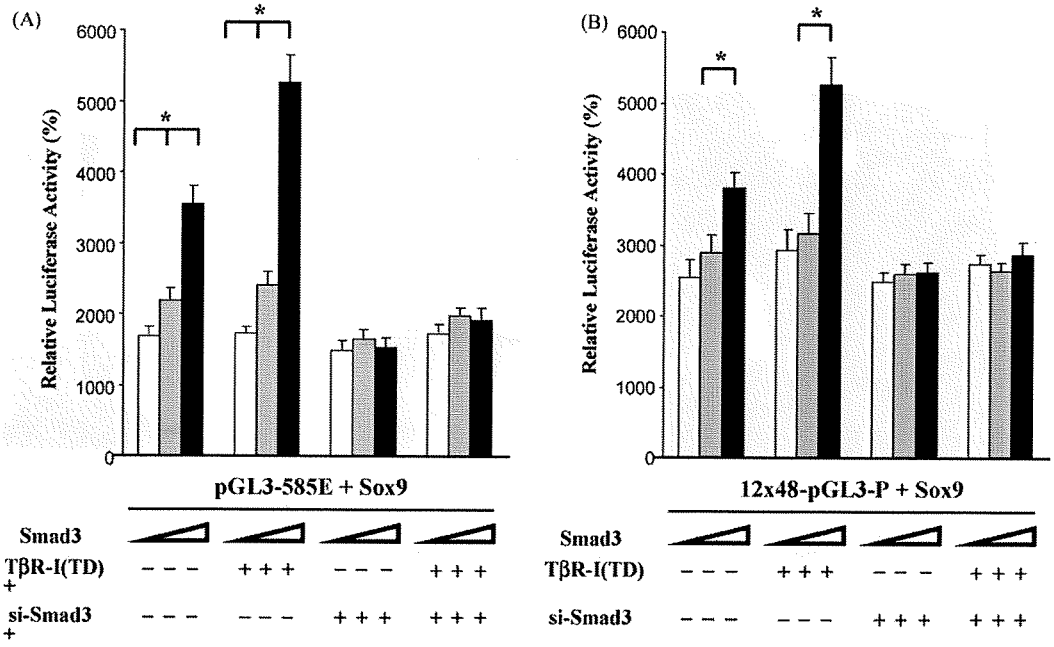

Fig. 2. Smad3 has an essential role for TGF-β-stimulated transactivation in the Sox9-regulated gene expression. (A) Smad3 enhanced the Sox9-dependent transcription in a dose-dependent manner. Smad3 and TβR-I(TD) synergistically increased the luciferase activity in pGL3-585E reporter systems. si-RNA against Smad3 (si-Smad3) totally inhibited the synergistic effects of Smad3 and TβR-I(TD). Note that si-Smad3 did not inhibit the Sox9-induced transactivation of reporter genes. (B) In 12 × 48 pGL3-P reporter systems, Smad3 and TβR-I(TD) cooperatively stimulated the relative luciferase activity up to 1.7-fold higher level in the presence of Sox9. A dose-dependent effect of Smad3 was observed. However, the increase of luciferase activity was suppressed by si-Smad3 in Smad3-transfected cells. Relative luciferase activities were calculated using the activity of pGL3-B (A) or pGL3-P (B) as a control (100%). Triangular boxes denote the transfection volume of Smad3 expression plasmid (0, 25, and 50 ng). *Statistical significances ($p < 0.05$) were observed between the indicated bars with the Mann–Whitney *U*-test. Error bars, S.D.

3.3. Recombinant Sox9 associates with p300 and binds to the Col2a1 enhancer in vitro

To examine the role of Sox9-associated transcriptional complex (Sox9, p300, and Smad3) on chromatin, we purified histones from HeLa cells, chromatin assembly-related molecules (NAP-1 and ACF complex), Sox9, p300, and Smad3 as described in Section 2. Purified NAP-1 and ACF sufficiently assembled chromatin under histone-containing conditions. Chromatin assembling abilities of these molecules were estimated by MNase digestion assays (Fig. 3A). Recombinant Sox9 purified from Sf9 cells associated with recombinant p300 in vitro (Fig. 3B). Recombinant Sox9 also bound with high affinity to the Col2a1 enhancer probe, which contains the Sox9-binding sequence, in EMSA (Fig. 3C).

3.4. TGF-β-stimulated Smad3 and p300 cooperatively activate the Sox9-dependent transcription on chromatin

For in vitro transcription analyses after chromatin assembly (Fig. 4A), we assessed the complex formation of Smad3 and Smad4. Smad3 purified from the nuclear fraction of TGF-β-treated Sf9 cells was a phosphorylated form of Smad3 (Fig. 4B). Smad4 was also detected in the same coimmunoprecipitated fraction using anti-FLAG M2 affinity gel (Fig. 4B). This result demonstrated that phosphorylated Smad3 was transferred into the nucleus with Smad4 by TGF-β treatment. In addition, purified Smad3/4 associated with recombinant Sox9 and p300 in vitro (Fig. 4C). Here we investigated the effect of phosphorylated Smad3 in the Sox9-dependent transcription on chromatin. In vitro transcription analyses on chromatinized templates revealed that the combination of Sox9, Smad3/4, and p300 were necessary for the activation of chromatin-mediated transcription (Fig. 4D). These findings suggest that the Sox9-dependent chondrogenesis might be strictly controlled by TGF-β signal Smad3 and chromatin remodeling factor p300.

4. Discussion

The present study indicates that TGF-β receptor-regulated Smad3 and p300 cooperatively activate the Sox9-dependent transcription on chromatin. The TGF-β signal plays an essential role to induce primary chondrogenesis (Pittenger et al., 1999; Heng et al., 2004). However, the differentiation of chondrocyte is regulated by the conflictive effects of TGF-β. TGF-β3 enhances the early chondrogenesis derived from mesenchymal stem cells (Fan et al., 2008). The short-term treatment with TGF-β3 has been reported to maintain a chondrogenic phenotype (Mehlhorn et al., 2006). On the other hand, TGF-β inhibits chondrocyte maturation at the late stage (Ballock et al., 1993; Ferguson et al., 2000). We previously described that TGF-β signal Smad3 promotes the early chondrogenesis through the activation of Sox9 (Furumatsu et al., 2005a). However, the cross-talk between TGF-β signal and Sox9 in the epigenetic regulation for initiating chondrogenesis is still unclear. Here, we further analyzed a crucial role of Smad3 in the Sox9-dependent chondrogenesis on chromatin. In this study, Smad3 enhanced the Sox9-mediated transcription in luciferase reporter assay systems (Fig. 1B and C). The increase of relative luciferase activity with Smad3 was higher in pGL3-585E, which contains a native set of Col2a1 promoter and enhancer, than in 12 × 48-pGL3-P systems. These findings might be caused by the binding affinity of Sox9 against each reporter plasmid. The activity of 12 × 48-pGL3-P containing high copies of Sox9-binding site might be already excited by the cotransfection of Sox9. A dose-dependent transactivation by Smad3 was observed in both systems,

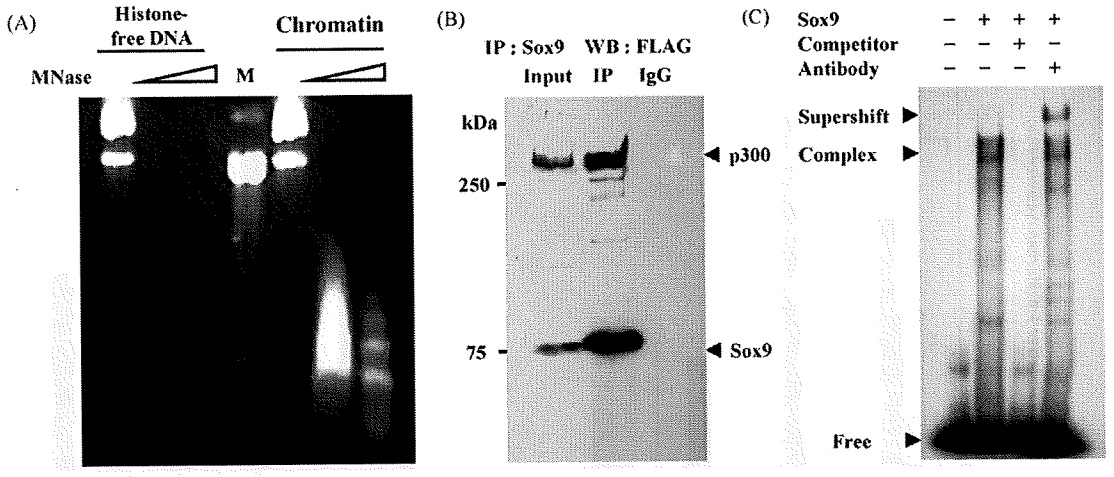

Fig. 3. MNase digestion analyses after chromatin assembly. Purified Sox9 form a complex with p300 or DNA probe containing the Sox9-binding site. (A) Closed circular 12 × 48-pGL3-P (300 ng) was used as a template. Chromatin assembling steps were performed as shown in Fig. 4A. Plasmid DNAs were completely digested by MNase (0.02 and 0.04 U/15 μl) in the absence of histones, NAP-1, and ACF (Histone-free DNA). Chromatinized plasmids were protected from complete digestion (Chromatin). Nucleosome-repeated pattern (approximately 165 bp) was observed in chromatin template after MNase treatment (0.04 U/15 μl). M, 123-bp ladder (Invitrogen). (B) Purified p300 was coimmunoprecipitated with recombinant Sox9 using anti-Sox9 antibody. Western blotting was performed with anti-FLAG M2 antibody. Sox9 (30 ng) was incubated with p300 (30 ng), and then the 10% of reaction was loaded as an input. Immunoprecipitation using rabbit IgG was performed as a control. Numbers indicate molecular weight (kDa). (C) Purified Sox9 associated with the Col2a1 enhancer probe in EMSA. The unlabeled competitor decreased the signal of Sox9–DNA complex. Supershifted band was observed in the presence of anti-Sox9 antibody.

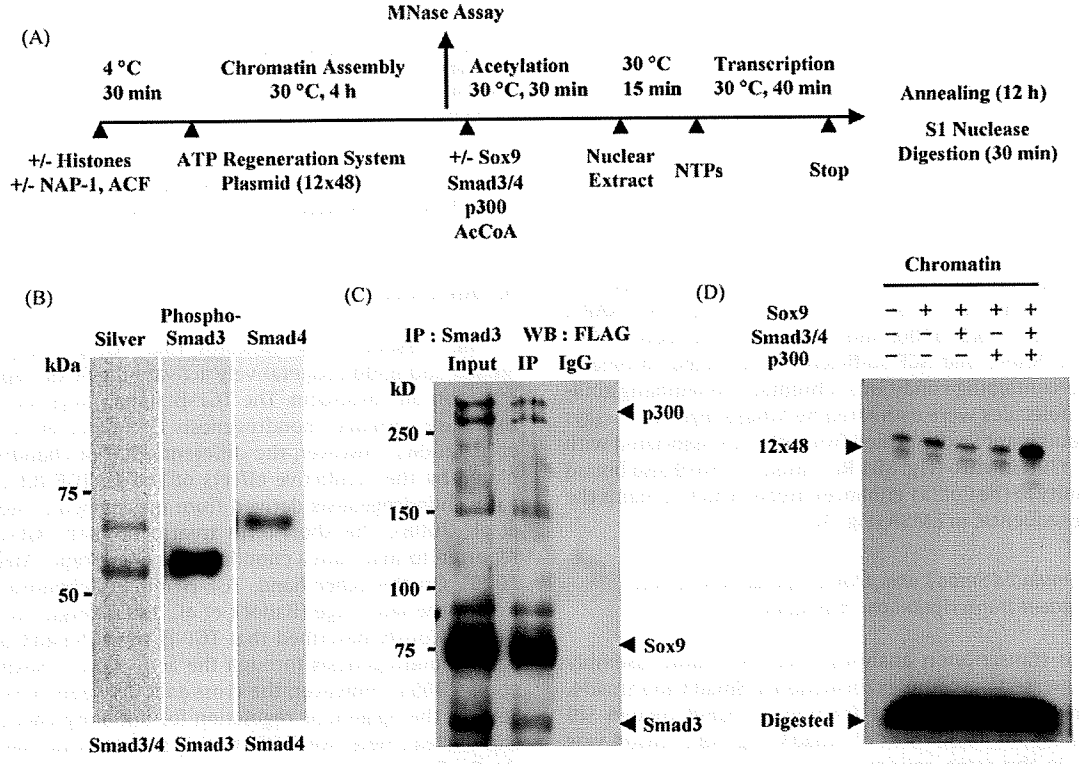

Fig. 4. Phosphorylated Smad3 and p300 cooperatively activate the Sox9-dependent transcription on chromatin. (A) The sequential steps for chromatin assembly and in vitro transcription are illustrated. MNase assays were performed after chromatin assembly (Fig. 3A). To estimate the amounts of RNAs transcribed from chromatinized plasmid, S1 nuclease assays were performed as described in Section 2. S1 nuclease digests a single-stranded part of RNA and excessive primers. Remaining double-stranded fragments (49-bp), which are annealed with ^{32}P end-labeled specific primers, represent transcriptional activities on chromatin. (B) Recombinant Smad3/4 were prepared using baculovirus expression systems. The details are described in Section 2. Smad3/4 complex were visualized with silver staining (left lane). Phosphorylated Smad3 were obtained after TGF-β treatments (middle lane). Smad4 was coimmunoprecipitated with FLAG-tagged Smad3 (right lane). (C) Protein–protein interactions among recombinant proteins. Purified Sox9 (50 ng), p300 (50 ng), and Smad3/4 (50/15 ng) were incubated, and then immunoprecipitated with anti-Smad2/3 antibodies. Sox9 and p300 were coimmunoprecipitated with Smad3 (IP). Western blotting analyses were performed with anti-FLAG M2 antibodies. (D) Sox9, Smad3/4, and p300 cooperatively enhanced the transcriptional activities of chromatinized 12 × 48-pGL3-P (12 × 48, upper bands). Chromatin-mediated transcription was not fully activated by the combined treatment with Sox9 and Smad3/4 (or p300). Note that the synergistic effect of triple combination with Sox9, Smad3/4, and p300 was observed (right lane). Digested denotes non-annealed probes, which were digested by S1 nuclease treatments (lower bands).

and was totally suppressed by the cotransfection of si-RNA against Smad3 itself (Fig. 2). We previously demonstrated that si-Smad3 completely decreased the Col2a1 expression in a mesenchymal stem cell-derived chondrogenic model (Furumatsu et al., 2005a). These results suggest that Smad3 is the major transducer of TGF-β signal in the Sox9-regulated early chondrogenesis.

The Sox9-dependent transcription is synergistically activated by p300 on chromatin (Furumatsu et al., 2005b). Transcriptional coactivator p300 has an important role for gene expression and cellular differentiation (Dilworth et al., 2004; Espinosa and Emerson, 2001; Kitagawa et al., 2003). The effect of p300 is exerted through several mechanisms. p300 acts as a protein scaffold and a bridging factor for forming transcriptional complexes. In addition, the intrinsic histone acetyltransferase activity of p300 has a potential to facilitate the transcriptional activity by modulating chromatin structure (Chan and La Thangue, 2001; Korzus et al., 1998; Utley et al., 1998). Several authors have reported that p300 plays a critical role for the activation of cAMP response element-binding protein-, MyoD-, p53-, or vitamin D receptor-dependent transcription on reconstituted chromatin (Asahara et al., 2001; Dilworth et al., 2004; Espinosa and Emerson, 2001; Kitagawa et al., 2003). In previous studies, we described that p300 and Smad3 enhanced the Sox9-dependent transcription by associating with Sox9 (Tsuda et al., 2003; Furumatsu et al., 2005a). However, the precise effect of the third associating factor, such as Smad3, on chromatin is still unclear. To analyze the additional effect of the third factor in a chromatin assembly model is considered to be hard. This study revealed the additional effect of phosphorylated Smad3 in the Sox9- and p300-mediated transcription using 12 × 48-pGL3-P-based chromatin assembly model (Fig. 4D). However, the synergistic effect of Smad3 was not observed in a different balance of Sox9-associating molecules (data not shown). In pGL3-585E systems, we could not detect a significant effect of Smad3 on chromatin-derived transcription, either (data not shown). These findings suggest that the balance of Sox9-associating factors and the accessibility to chromatinized promoter might be important for the epigenetic regulation of chondrogenesis. In addition, the discrepancy of Smad3-induced transactivation between reporter assays (Figs. 1 and 2) and chromatin-derived transcription (Fig. 4D) might be caused by the following reasons: (i) the chromatinized status of Sox9-reactive plasmid was different in each analysis, (ii) the influence of Sox9 and p300 was more critical on chromatin-assembled plasmid, and (iii) unknown factors in SW1353 nuclear extracts might have important roles in the Sox9-dependent transcription on chromatin. Several transcription partners such as Sox-5/6, PGC-1α, Barx2, and TRAP230 can modify the Sox9-dependent transcription during chondrogenesis (Ikeda et al., 2004; Kawakami et al., 2005; Lefebvre et al., 2001; Meech et al., 2005; Zhou et al., 2002). Further analyses to identify the other unknown partners of Sox9-based transcriptional complex will be required.

Animal models for a loss of Smad3 function have revealed the importance of Smad3 in physiological systems. Smad3 null mice show skeletal defects including osteoarthritis (Datto et al., 1999). Haploinsufficiency of Smad2 and Smad3 causes an embryonic lethality due to endodermal defects and exhibits craniofacial defects (Liu et al., 2004). We previously reported that Smad3 had an important role for primary chondrogenesis (Furumatsu et al., 2005a). In addition to the Smad3 pathway, TGF-β activates mitogen-activated protein kinase (MAPK) pathway during chondrogenic differentiation (Stanton et al., 2003). Several authors have shown that MAPK pathway modulates Col2a1 and Sox9 expression in chondrogenesis (Murakami et al., 2000; Nakamura et al., 1999; Tuli et al., 2003). These reports suggest that TGF-β-stimulated MAPK pathway would also be involved in chondrogenesis with modifying the Sox9-dependent transcription. Further studies to analyze the relationships between MAPK pathway and the Sox9-mediated transcription on chromatin are required.

In conclusion, the present study demonstrates that Smad3 enhances the Sox9-dependent transcription on chromatin. Our findings suggest the potential molecular mechanism how TGF-β signals induce early chondrogenesis via chromatin regulation.

Acknowledgements

We thank B. de Crombrugghe, T. Imamura, T. Ito, Y. Yamada, and TP. Yao for providing us with plasmids and baculovirus. We are also grateful to M. Lotz and our colleagues at the Department of Molecular and Experimental Medicine for their great support during this study.

This work was supported in part by grants from NIH (AR50631), JST SORST, Genome Network Project (MEXT), Grants-in Aid for Scientific Research (MEXT), Research on Child Health and Development, Research on Publicly, Essential Drugs and Medical Device (Japan Health Sciences Foundation) (H.A.), Japan Society for the Promotion of Science (grant-in-aid for scientific research 18890115 and 20791040), and Japanese Foundation for Research and Promotion of Endoscopy, and by a fellowship conferred from Uehara Memorial Foundation (T.F.).

Appendix A. Supplementary data

Supplementary data associated with this article can be found, in the online version, at doi:10.1016/j.biocel.2008.10.032.

References

Akiyama H, Chaboissier MC, Martin JF, Schedl A, de Crombrugghe B. The transcription factor Sox9 has essential roles in successive steps of the chondrocyte differentiation pathway and is required for expression of Sox5 and Sox6. Genes Dev 2002;16:2813–28.

Akiyama H, Lyons JP, Mori-Akiyama Y, Yang X, Zhang R, Zhang Z, et al. Interactions between Sox9 and β-catenin control chondrocyte differentiation. Genes Dev 2004;18:1072–87.

Asahara H, Santoso B, Guzman E, Du K, Cole PA, Davidson I, et al. Chromatin-dependent cooperativity between constitutive and inducible activation domains in CREB. Mol Cell Biol 2001;21:7892–900.

Asahara H, Tartare-Deckert S, Nakagawa T, Ikehara T, Hirose F, Hunter T, et al. Dual roles of p300 in chromatin assembly and transcriptional activation in cooperation with nucleosome assembly protein 1 in vitro. Mol Cell Biol 2002;22:2974–83.

Ballock RT, Heydemann A, Wakefield LM, Flanders KC, Roberts AB, Sporn MB. TGF-β 1 prevents hypertrophy of epiphyseal chondrocytes: regulation of gene expression for cartilage matrix proteins and metalloproteases. Dev Biol 1993;158:414–29.

Bell DM, Leung KK, Wheatley SC, Ng LJ, Zhou S, Ling KW, et al. SOX9 directly regulates the type-II collagen gene. Nat Genet 1997;16:174–8.

Chan HM, La Thangue NB. p300/CBP proteins: HATs for transcriptional bridges and scaffolds. J Cell Sci 2001;114:2363–73.

Datto MB, Frederick JP, Pan L, Borton AJ, Zhuang Y, Wang XF. Targeted disruption of Smad3 reveals an essential role in transforming growth factor beta-mediated signal transduction. Mol Cell Biol 1999;19:2495–504.

Dilworth FJ, Seaver KJ, Fishburn AL, Htet SL, Tapscott SJ. In vitro transcription system delineates the distinct roles of the coactivators pCAF and p300 during MyoD/E47-dependent transactivation. Proc Natl Acad Sci USA 2004;101:11593–8.

Espinosa JM, Emerson BM. Transcriptional regulation by p53 through intrinsic DNA/chromatin binding and site-directed cofactor recruitment. Mol Cell 2001;8:57–69.

Fan H, Zhang C, Li J, Bi L, Qin L, Wu H, et al. Gelatin microspheres containing TGF-β3 enhance the chondrogenesis of mesenchymal stem cells in modified pellet culture. Biomacromolecules 2008;9:927–34.

Felsenfeld G, Groudine M. Controlling the double helix. Nature 2003;421:448–53.

Ferguson CM, Schwarz EM, Reynolds PR, Puzas JE, Rosier RN, O'Keefe RJ. Smad2 and 3 mediate transforming growth factor-β1-induced inhibition of chondrocyte maturation. Endocrinology 2000;141:4728–35.

Furumatsu T, Tsuda M, Taniguchi N, Tajima Y, Asahara H. Smad3 induces chondrogenesis through the activation of SOX9 via CREB-binding protein/p300 recruitment. J Biol Chem 2005a;280:8350–843.

Furumatsu T, Tsuda M, Yoshida K, Taniguchi N, Ito T, Hashimoto M, et al. Sox9 and p300 cooperatively regulate chromatin-mediated transcription. J Biol Chem 2005b;280:35203–8.

Heldin CH, Miyazono K, ten Dijke P. TGF-β signalling from cell membrane to nucleus through SMAD proteins. Nature 1997;390:465–71.
Heng BC, Cao T, Lee EH. Directing stem cell differentiation into the chondrogenic lineage in vitro. Stem Cells 2004;22:1152–67.
Ikeda T, Kamekura S, Mabuchi A, Kou I, Seki S, Takato T, et al. The combination of SOX5, SOX6, and SOX9 (the SOX trio) provides signals sufficient for induction of permanent cartilage. Arthritis Rheum 2004;50:3561–73.
Ito T, Bulger M, Kobayashi R, Kadonaga JT. Drosophila NAP-1 is a core histone chaperone that functions in ATP-facilitated assembly of regularly spaced nucleosomal arrays. Mol Cell Biol 1996;16:3112–24.
Ito T, Levenstein ME, Fyodorov DV, Kutach AK, Kobayashi R, Kadonaga JT. ACF consists of two subunits, Acf1 and ISWI, that function cooperatively in the ATP-dependent catalysis of chromatin assembly. Genes Dev 1999;13:1529–39.
Ito T, Ikehara T, Nakagawa T, Kraus WL, Muramatsu M. p300-mediated acetylation facilitates the transfer of histone H2A-H2B dimers from nucleosomes to a histone chaperone. Genes Dev 2000;14:1899–907.
Jaenisch R, Bird A. Epigenetic regulation of gene expression: how the genome integrates intrinsic and environmental signals. Nat Genet 2003;33(Suppl):245–54.
Kawakami Y, Tsuda M, Takahashi S, Taniguchi N, Esteban CR, Zemmyo M, et al. Transcriptional coactivator PGC-1α regulates chondrogenesis via association with Sox9. Proc Natl Acad Sci USA 2005;102:2414–9.
Kitagawa H, Fujiki R, Yoshimura K, Mezaki Y, Uematsu Y, Matsui D, et al. The chromatin-remodeling complex WINAC targets a nuclear receptor to promoters and is impaired in Williams syndrome. Cell 2003;113:905–17.
Korzus E, Torchia J, Rose DW, Xu L, Kurokawa R, McInerney EM, et al. Transcription factor-specific requirements for coactivators and their acetyltransferase functions. Science 1998;279:703–7.
Lefebvre V, Behringer RR, de Crombrugghe B. L-Sox5, Sox6 and Sox9 control essential steps of the chondrocyte differentiation pathway. Osteoarthritis Cartilage 2001;9:S69–75.
Li E. Chromatin modification and epigenetic reprogramming in mammalian development. Nat Rev Genet 2002;3:662–73.
Liu Y, Festing M, Thompson JC, Hester M, Rankin S, El-Hodiri HM, et al. Smad2 and Smad3 coordinately regulate craniofacial and endodermal development. Dev Biol 2004;270:411–26.
Meech R, Edelman DB, Jones FS, Makarenkova HP. The homeobox transcription factor Barx2 regulates chondrogenesis during limb development. Development 2005;132:2135–46.
Mehlhorn AT, Niemeyer P, Kaiser S, Finkenzeller G, Stark GB, Südkamp NP, et al. Differential expression pattern of extracellular matrix molecules during chondrogenesis of mesenchymal stem cells from bone marrow and adipose tissue. Tissue Eng 2006;12:1393–403.
Murakami S, Kan M, McKeehan WL, de Crombrugghe B. Up-regulation of the chondrogenic Sox9 gene by fibroblast growth factors is mediated by the mitogen-activated protein kinase pathway. Proc Natl Acad Sci USA 2000;97:1113–8.
Nakagawa T, Bulger M, Muramatsu M, Ito T. Multistep chromatin assembly on supercoiled plasmid DNA by nucleosome assembly protein-1 and ATP-utilizing chromatin assembly and remodeling factor. J Biol Chem 2001;276:27384–91.
Nakamura K, Shirai T, Morishita S, Uchida S, Saeki-Miura K, Makishima F. p38 mitogen-activated protein kinase functionally contributes to chondrogenesis induced by growth/differentiation factor-5 in ATDC5 cells. Exp Cell Res 1999;250:351–63.
Ng LJ, Wheatley S, Muscat GE, Conway-Campbell J, Bowles J, Wright E, et al. SOX9 binds DNA, activates transcription, and coexpresses with type II collagen during chondrogenesis in the mouse. Dev Biol 1997;183:108–21.
Pittenger MF, Mackay AM, Beck SC, Jaiswal RK, Douglas R, Mosca JD, et al. Multilineage potential of adult human mesenchymal stem cells. Science 1999;284:143–7.
Shi Y, Massagué J. Mechanisms of TGF-β signaling from cell membrane to the nucleus. Cell 2003;113:685–700.
Stanton LA, Underhill TM, Beier F. MAP kinases in chondrocyte differentiation. Dev Biol 2003;263:165–75.
Stricker S, Fundele R, Vortkamp A, Mundlos S. Role of Runx genes in chondrocyte differentiation. Dev Biol 2002;245:95–108.
Tsuda M, Takahashi S, Takahashi Y, Asahara H. Transcriptional co-activators CREB-binding protein and p300 regulate chondrocyte-specific gene expression via association with Sox9. J Biol Chem 2003;278:27224–9.
Tuli R, Tuli S, Nandi S, Huang X, Manner PA, Hozack WJ, et al. Transforming growth factor-β-mediated chondrogenesis of human mesenchymal progenitor cells involves N-cadherin and mitogen-activated protein kinase and Wnt signaling cross-talk. J Biol Chem 2003;278:41227–36.
Utley RT, Ikeda K, Grant PA, Cote J, Steger DJ, Eberharter A, et al. Transcriptional activators direct histone acetyltransferase complexes to nucleosomes. Nature 1998;394:498–502.
Zhou R, Bonneaud N, Yuan CX, de Santa Barbara P, Boizet B, Schomber T, et al. SOX9 interacts with a component of the human thyroid hormone receptor-associated protein complex. Nucleic Acids Res 2002;30:3245–52.

Mod Rheumatol (2009) 19:273–282
DOI 10.1007/s10165-009-0170-4

ORIGINAL ARTICLE

A combination of biochemical markers of cartilage and bone turnover, radiographic damage and body mass index to predict the progression of joint destruction in patients with rheumatoid arthritis treated with disease-modifying anti-rheumatic drugs

Jun Hashimoto · Patrick Garnero · Désirée van der Heijde · Nobuyuki Miyasaka · Kazuhiko Yamamoto · Shinichi Kawai · Tsutomu Takeuchi · Hideki Yoshikawa · Norihiro Nishimoto

Received: 26 December 2008 / Accepted: 10 March 2009 / Published online: 19 May 2009

Abstract The aim of this study was to evaluate the predictive value of biological, radiological and clinical parameters for the progression of radiographic joint damage in rheumatoid arthritis (RA) patients treated with conventional disease-modifying anti-rheumatic drugs (DMARDs). We analyzed the 145 patients with active RA for less than 5 years who were participating in the prospective 1-year randomized controlled trial of tocilizumab (SAMURAI trial) as a control arm treated with conventional DMARDs. Progression of joint damage was assessed by sequential radiographs read by two independent blinded X-ray readers and scored for bone erosion and joint space narrowing (JSN) using the van der Heijde-modified Sharp method. Multivariate analysis revealed that increased urinary levels of C-terminal crosslinked telopeptide of type II collagen (U-CTX-II), an increased urinary total pyridinoline/total deoxypyridinoline (U-PYD/DPD) ratio and low body mass index (BMI) at baseline were independently associated with a higher risk for progression of bone erosion. In addition to these three variables, the JSN score at baseline was also significantly associated with an increased risk of progression of the JSN score and total Sharp score. High baseline U-CTX-II levels, U-PYD/DPD ratio and JSN score and a low BMI are independent predictive markers for the radiographically evident joint damage in patients with RA treated with conventional DMARDs.

Keywords BMI · CTX-II · Joint destruction · PYD/DPD ratio · Rheumatoid arthritis

J. Hashimoto · H. Yoshikawa
Osaka University Graduate School of Medicine, Osaka, Japan

P. Garnero
Inserm Research Unit 664 and Synarc, Lyon, France

D. van der Heijde
Leiden University Medical Center, Leiden, The Netherlands

N. Miyasaka
Tokyo Medical and Dental University, Tokyo, Japan

K. Yamamoto
The University of Tokyo, Tokyo, Japan

S. Kawai
Toho University Omori Medical Center, Tokyo, Japan

T. Takeuchi
Saitama Medical Center/School, Saitama, Japan

N. Nishimoto (✉)
Laboratory of Immune Regulation, Wakayama Medical University, 105 Saito Bio Innovation Center, 7-7-20 Saito-Asagi, Ibaraki, Osaka 565-0085, Japan
e-mail: norichan@wakayama-med.ac.jp

Introduction

Although rheumatoid arthritis (RA) has features of a systemic disease and capable of exhibiting a variety of extra-articular manifestations, it is predominantly characterized by structural destruction of the joints, leading to functional disability [1–4]. Joint destruction often progresses early in the disease process [5–8], but the process is highly variable from patient to patient [9–12]. The identification of patients with rapid joint destruction very early in the disease process is of critical importance to clinicians wanting to optimize treatment strategies. Indeed, although new biological therapies are highly effective in preserving joint structure, they are expensive and may have side effects.

Thus, targeting these treatments to RA patients manifesting rapid progression of the disease may be beneficial.

Several prospective studies have been performed to identify predictive factors indicative of a worse radiological progression of RA [13–31]. The earlier investigations revealed the importance of the rheumatoid factor (RF), inflammation markers or radiographic damage at baseline [13, 14, 16–18, 20, 21], while more recent ones have identified biochemical markers of bone, cartilage and synovial tissue metabolism and catabolic enzymes as being associated with progression in RA [15, 19, 22, 24, 27–29]. Alternatively, RA is also associated with accelerated atherosclerosis and increased cardiovascular mortality and, recently, it has been shown that macrophage inhibitory cytokine 1 (MIC-1), which is linked to clinical events in atherosclerosis, may be involved in the pathological process of erosive joint destruction [32]. The body mass index (BMI) has also been reported to be associated with the radiographic progression of RA, independent of inflammation markers [23, 30, 31], and recent new information suggests the potential involvement of adipokines as regulators of inflammation in RA [33]. These new findings have lead to the recognition of RA as a disease involving a variety of pathological conditions related with joint destruction and made clinicians aware of the fact that RA is a systemic disease in terms of the pathology of the bone and destruction of cartilage. However, to date, there has been no study that has analyzed concomitantly in the same population the independent contribution of these various anthropometric, clinical, laboratory and radiological features to the prediction of disease progression in RA.

The aims of the study reported here were to determine which combination of a few risk factors identified among a panel of clinical, biological and radiological parameters would be powerful in predicting the radiological progression of bone erosion and joint space narrowing (JSN) in RA patients treated with conventional disease-modifying antirheumatic drugs (DMARDs).

Methods

Patients and protocol

The patient cohort consists of 148 patients with RA receiving conventional DMARDs who participated in the control arm of the SAMURAI trial described in a recent publication [34]. The aim of the SAMURAI, which was a 52-week-long multi-center clinical trial, was to evaluate the effect of tocilizumab on radiological joint damage. Three hundred and six patients with RA diagnosed according to the American College of Rheumatology criteria [35] were randomly assigned to tocilizumab monotherapy (8 mg/kg intravenously every 4 weeks) or conventional DMARDs. For the DMARDs group, the dose, type and combination of DMARDs and/or immunosuppressants could vary according to disease activity at the discretion of the treating physician. The study protocol was approved by the Ministry of Health, Labor and Welfare of Japan, and by the ethical committee at each participating site, and patients gave their written informed consent.

Radiographic assessment

Posteroanterior radiographs of hands and anteroposterior radiographs of feet were performed at baseline and at weeks 28 and 52 or at the last visit for patients who withdrew from the study prior to week 52. Radiographs were scored using the van der Heijde-modified Sharp method [36, 37] for bone erosion, joint space narrowing (JSN) and total sharp score (TSS) independently by two readers who were well trained and competent to score radiographs in accordance with the method. The readers were blinded to the treatment group and chronological order of the films.

Clinical assessment

The Disease Activity Score on 28 joints (DAS28), clinical improvement in signs and symptoms of RA, tender joint count, swollen joint count, and modified health assessment questionnaire (MHAQ) [38] were assessed at baseline.

Laboratory examinations

Fasting blood samples and the second morning urine samples were obtained from all subjects at clinical visits. C-reactive protein (CRP) and erythrocyte sedimentation rate (ESR) were measured in the local clinical test laboratory of each investigation site.

To assess bone formation, we measured serum intact-osteocalcin (OC) using a two-site immunoradiometric assay (Mitsubishi Kagaku Iatron, Japan) and serum bone alkaline phosphatase (bone ALP) by an enzyme-linked immunosorbent analysis (ELISA; Quidel, San Diego, CA). Markers of bone resorption included urinary N-terminal crosslinked telopeptide of type I collagen (U-NTX-I), which was measured by an ELISA (Ostex Int, Seattle, WA), and urinary total deoxypyridinoline (U-DPD) and total pyridinoline (U-PYD), measured by a high-performance liquid chromatography (HPLC) assay. Markers of cartilage synthesis included the N-terminal propeptide of type IIA collagen (PIIANP; Linco, St. Louis, MO) and the C-terminal propeptide of type II collagen (PIICP; IBEX Diagnostics, Montreal, Canada). Cartilage degradation was assessed by the urinary excretion of the C-terminal

crosslinked telopeptide of type II collagen (CTX-II Carti-Laps ELISA; NORDIC Biosciences, Herlev, Denmark). Synovial tissue metabolism was assessed by measuring the urinary excretion of glucosyl–galactosyl–pyridinoline (Glc–Gal–PYD) by HPLC, serum matrix metalloproteinase-3 (MMP-3) by ELISA (Daiichi Pure Chemical, Japan) and serum amyloid protein A (SAA) by a latex immunoassay (LIA; Eiken Chemical, Japan). Other measures included serum interleukin-6 (IL-6) using a chemiluminescent enzyme immunoassay (CLEIA) (Fujirebio Japan), RF by LIA (Mitsubishi Kagaku Iatron, Japan), and immunoglobulin G (IgG) by LIA (Eiken Chemical, Japan).

Statistical analysis

For analyzing the correlation between markers at baseline and at the 52-week radiological progression of joint damage, we normalized the markers by logarithmic transformation when needed. First, the markers were selected by Pearson correlation coefficient with TSS, erosion score, and JSN score ($|r| > 0.15$). Then, the predictive factors were selected based on the multivariate regression analysis using the backward elimination method, the forward selection method, and the best-subset selection procedure using Mallows' Cp- adjusted R^2.

The odds ratio of progression in TSS, bone erosion and JSN score according to the levels of these baseline factors were estimated by logistic regression analysis with a 95% confidence interval (95% CI). The progression of joint damage was defined as an increase of TSS of 0.5 or more at 52 weeks.

All statistical analyses were two-sided, and p values <0.05 were considered to be significant. All statistical analyses were carried out using SAS ver. 8.2, TS2MO (SAS Institute, Cary, NC).

Results

One hundred and forty-five patients were included in the intent to treatment (ITT) analyses. Demographics and baseline disease characteristics are shown in Tables 1 and 3. At baseline, the mean age and the disease duration were 53.1 and 2.4 years, respectively. Patients had very active disease, as indicated by a DAS28 score of 6.4 and CRP of 4.9 mg/dl at baseline. The kinds of DMARDs and immunosuppressants used for RA treatment during the study and the number of patients are shown in Table 2.

Bivariate linear correlation analyses showed that baseline values of U-PYD, the ratio U-PYD/DPD, U-CTX-II, U–Glc–Gal–PYD, TSS, erosion score, JSN score, age and BMI were associated significantly with the 1-year increase in all three radiological indices of joint damage, i.e. bone erosion score, JSN score and TSS (Table 3). The baseline levels of U-DPD, S-PIIANP, triglyceride, ferritin also had a significant association with one or two variables among these three radiographic progression parameters (Table 3). None of the clinical indices of disease activity nor the biological parameters of inflammation were associated significantly with radiological progression. In the

Table 1 Baseline demographics, clinical and laboratory characteristics of the patient cohort

Baseline demographics, clinical and laboratory characteristics	Values
Number of patients	145
Age, years (mean)	53.1 ± 12.5
Female, *n* (%)	119 (82.1)
BMI (kg/m^2)	21.8 ± 3.0
RA duration (years)	2.4 ± 1.3
Number of previous DMARDs	2.8
Tender joint count	14.4 ± 7.5
Swollen joint count	11.8 ± 5.8
CRP (mg/dl)	4.9 ± 2.9
DAS28	6.4 ± 0.9
Radiological total Sharp score	30.6 ± 42.0
Radiological bone erosion score	13.9 ± 21.7
Radiological joint space narrowing (JSN) score	16.7 ± 21.8

Values are given as the mean ± standard deviation, unless otherwise indicated

RA Rheumatoid arthritis, *DAS28* Disease Activity Score based on 28 joint counts, *CRP* C-reactive protein, *BMI* body mass index, *DMARDs* disease-modifying anti-rheumatic drugs

Table 2 Number of patients using concomitant drugs related to rheumatoid arthritis during the study

Variables	Number of patients[a]
Corticosteroids	145 (100%)
Methotrexate	123 (84.8%)
Mizoribine	11 (7.6%)
Azathioprine	7 (4.8%)
Ciclosporin	5 (3.4%)
Tacrolimus hydrate	3 (2.1%)
Sulfasalazine	60 (41.4%)
Bucillamine	33 (22.8%)
Sodium aurothiomalate	4 (2.8%)
D–Penicillamine	11 (7.6%)
Actarit	6 (4.1%)
Lobenzarit disodium	2 (1.4%)
Cyclophosphamide	2 (1.4%)
Minocycline hydrochloride	2 (1.4%)

[a] Values are given as the number of patients taking a drug; patients can take more than one drug

Table 3 Baseline patient measurements and Pearson correlation coefficient between the levels of candidate factors at baseline and the changes in radiographic score at week 52

Variables	Levels at baseline (mean ± SD)	*r* value between baseline levels and radiological progression at week 52		
		Total sharp score	Bone erosion score	Joint space narrowing (JSN) score
Bone markers				
Intact-osteocalcin (ng/ml)	5.1 ± 2.1	NS	NS	NS
Bone alkaline phosphatase (U/l)	21.5 ± 6.5	NS	NS	NS
S-NTX-I (nmol BCE/l)	15.8 ± 4.8	NS	NS	NS
U-NTX-I (nmol BCE/mmol creatinine)	62.6 ± 31.9	NS	NS	NS
U-DPD (μmol/mol creatinine)	8 ± 4	0.185*	NS	0.187*
Bone or cartilage markers				
U-PYD (μmol/mol creatinine)	55 ± 37	0.278**	0.253**	0.274**
U-PYD/DPD	7.2 ± 1.8	0.190*	0.180*	0.178*
Cartilage markers				
S-PIIANP (ng/ml)	459.8 ± 210.9	NS	−0.188*	NS
S-PIICP (ng/ml)	819.1 ± 311.6	NS	NS	NS
U-CTX-II (ng/mmol creatinine)	902.5 ± 919.2	0.356***	0.321***	0.356***
Radiographic scores				
Total Sharp score	16.7 ± 21.8	0.323***	0.303***	0.307***
Erosion score	30.6 ± 42.0	0.313***	0.308***	0.282**
Joint space narrowing score	13.9 ± 21.7	0.323***	0.291***	0.322***
Symptoms or functions				
DAS28	6.4 ± 0.9	NS	NS	NS
Objective signs				
Tender joint count	14.4 ± 7.5	NS	NS	NS
Swollen joint count	11.8 ± 5.8	NS	NS	NS
Patients reported functional assessment				
MHAQ	0.90 ± 0.58	NS	NS	NS
Inflammation markers				
CRP (mg/dl)	4.9 ± 2.9	NS	NS	NS
ESR (mm/h)	71 ± 25	NS	NS	NS
MMP-3 (ng/ml)	456.5 ± 347.5	NS	NS	NS
SAA (μg/ml)	347 ± 307	NS	NS	NS
Fibrinogen (mg/dl)	490 ± 96	NS	NS	NS
Interleukin-6 (pg/ml)	60.2 ± 64.9	NS	NS	NS
Synovium degradation marker				
U-Glc–Gal–PYD (nmol/mmol creatine)	11.6 ± 9.3	0.255**	0.238**	0.245**
Hematological parameters				
WBC (/μl)	8,923 ± 2,430	NS	NS	NS
RBC (10^4/μl)	397 ± 38	NS	NS	NS
Hemoglobin (g/dl)	11.3 ± 1.4	NS	NS	NS
Platelet (10^4/μl)	37.2 ± 10.1	NS	NS	NS
Lipid parameters				
Total cholesterol (mg/dl)	182 ± 33	NS	NS	NS
HDL cholesterol (mg/dl)	56 ± 14	NS	NS	NS
LDL cholesterol (mg/dl)	108 ± 27	NS	NS	NS
Triglyceride (mg/dl)	90 ± 35	−0.187*	−0.193*	NS
Other biomarkers				
RF (IU/ml)	247 ± 452	NS	NS	NS

Table 3 continued

Variables	Levels at baseline (mean ± SD)	*r* value between baseline levels and radiological progression at week 52		
		Total sharp score	Bone erosion score	Joint space narrowing (JSN) score
IgG (mg/dl)	1,697 ± 492	NS	NS	NS
Albumin (g/dl)	3.7 ± 0.3	NS	NS	NS
Ferritin (ng/ml)	105 ± 116	NS	−0.182*	NS
Age	53.1 ± 12.5	−0.259**	−0.278**	−0.205*
Gender (M:F)	26:119	NS	NS	NS
Duration of disease	2.4 ± 1.3	NS	NS	NS
Anthropometric factor				
BMI (kg/m^2)	21.8 ± 3.0	−0.298***	−0.257**	−0.311***

NS not significant, *S-NTX* Serum type I collagen cross-linked N-telopeptides, *U-NTX* urinary type I collagen cross-linked N-telopeptides, *U-DPD* urinary deoxypyridinoline, *U-PYD* urinary pyridinoline, *S-PIIANP* serum N-terminal propeptide of type IIA collagen, *S-PIICP* serum C-terminal propeptide of type II collagen, *U-CTX-II* urinary C-terminal telopeptide of type II collagen, *MHAQ* modified health assessment questionnaire, *ESR* erythrocyte sedimentation rate, *MMP-3* matrix metalloproteinase-3, *SAA* serum amyloid protein A, *U-Glc–Gal–PYD* urinary glucosyl–galactosyl–pyridinoline, *IgG* immunoglobulin G, *WBC* white blood cell, *RBC* red blood cell, *HDL cholesterol* high-density lipoprotein cholesterol, *LDL cholesterol* low-density lipoprotein cholesterol

* $p < 0.05$; ** $p < 0.01$; *** $p < 0.001$

Table 4 Multivariate regression analysis relating JSN U-CTX-II, U-PYD/DPD, or BMI to changes in the radiographic scores at 52 weeks

Baseline predictor	Parameter estimate		*p* value
Total Sharp score progression			
JSN	4.88		0.04
PYD/DPD	20.81		0.02
CTX-II	9.41		<0.01
BMI	−0.92		<0.01
R^2		0.24	<0.001
Bone erosion progression			
PYD/DPD	11.20		0.04
CTX-II	5.58		<0.01
BMI	−0.48		0.02
R^2		0.17	<0.001
Joint space narrowing progression			
JSN	2.37		0.04
PYD/DPD	9.62		0.02
CTX-II	4.56		<0.01
BMI	−0.46		<0.01
R^2		0.25	<0.001

JSN Joint space narrowing, *PYD/DPD* logarithmic transformed urinary pyridinoline/deoxypyridinoline ratio, *CTX-II* logarithmic transformed urinary C-terminal telopeptide of type II collagen

multivariate analyses, increased levels of U-CTX-II, an increased U-PYD/DPD ratio and decreased BMI were the only independent predictors of the progression of bone erosion (Table 4). Together, these three variables explained 17% of the interindividual variance in the progression of bone erosion. For the progression of JSN and TTS, baseline JSN was also an independent predictor in addition to U-CTX-II, the U-PYD/DPD ratio and BMI (Table 4).

Logistic regression analysis after the categorization of the four predictive variables with the cut-off value of 500 ng/mmol/creatinine in U-CTX-II, median level for the U-PYD/DPD ratio, two cut-off values of 18.5 and 25 kg/m^2, respectively, in BMI and a 0 or >0 score in JSN score at baseline showed that the odds ratio for a yearly increase of TSS >0.5 was 2.6- to 9.9-fold higher risk in the high-risk group than in patients with low risk levels (Fig. 1a); the respective figures for progression in erosion score and for progression in JSN were 2.8–4.8 and 1.8–20.0, respectively (Fig. 1b, c). Baseline levels in the categorized groups are shown in Table 5.

Discussion

Based on our analysis of a panel of several demographical, clinical and laboratory parameters of disease activity, we found that increased urinary CTX-II, a high PYD/DPD ratio and low BMI were independent predictors of radiological progression in bone erosion and TTS in patients with RA receiving conventional DMARDs and that baseline JSN was also an independent predictor of radiological progression in JSN and TTS. These results suggest that these factors should be useful in identifying patients at high risk.

The bivariate analyses revealed that the baseline levels of U-PYD, the U-PYD/DPD ratio, U-CTX-II, TSS, erosion score, JSN score, U-Glc–Gal–PYD, age and BMI were

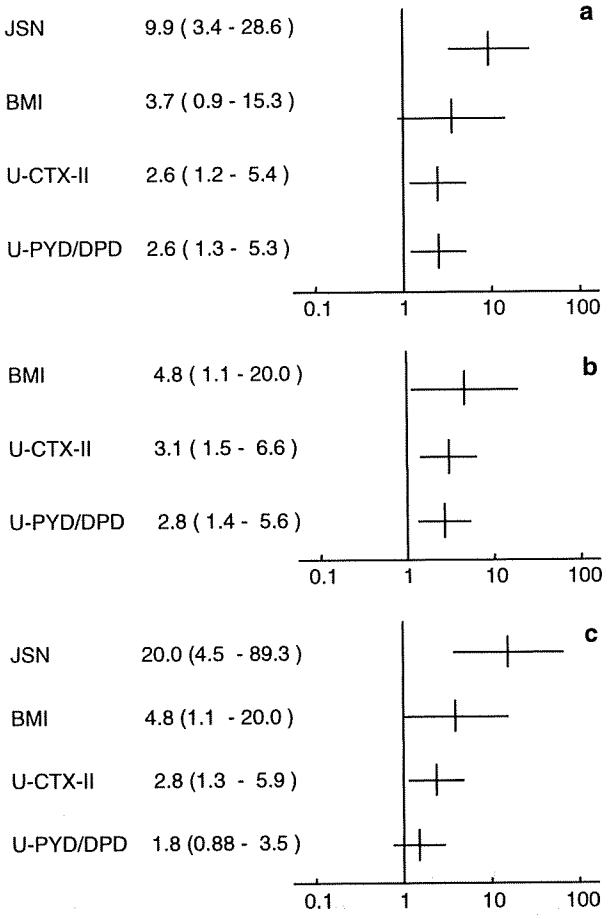

Fig. 1 Odds ratio (95% confidence interval) of radiological progression associated with high baseline joint space narrowing (*JSN*), high urinary C-terminal telopeptide of type II collagen (*U-CTXII*), high urinary total pyridinoline/total deoxypyridinoline (*U-PYD/DPD*), or low body mass index (*BMI*). Progression of joint damage over 1 year was defined as an increase >0.5 U of the total Sharp score (**a**), bone erosion (**b**) or JSN (**c**)

Table 5 Baseline levels in the categorized groups

Variables	Cut-off value	*n*	Mean of baseline value ± SD
JSN	0	30	0
	0<	115	21.1 ± 22.5
U-CTX-II (ng/mmol/creatinine)	<500	53	327.2 ± 104.6
	500≤	88	1,249.0 ± 1,014.9
U-PYD/DPD	<median (6.8)	72	5.8 ± 0.7
	Median (6.8)≤	73	8.6 ± 1.4
BMI (kg/m^2)	<18.5	20	17.5 ± 1.2
	18.5≤, <25	102	21.5 ± 1.6
	25≤	21	27.1 ± 1.7

significantly associated with the 1-year increase in all three indices of TSS, erosion score and JSN score and that the baseline levels of U-DPD, S-PIIANP, triglycerides and ferritin were significantly associated with one or two variables among these three radiographic progression parameters. However, there was no significant association with radiographic progression in the baseline levels of inflammation markers, MMP-3, hematological parameters, patients-reported functional assessments, such as MHAQ, and objective symptomatic scores. Although several previous studies showed that MMP-3 was predictive of radiological progression [22, 29, 39, 40] in RA, our data and those of Cunnane et al. [41] failed to reveal a significant association. Circulating MMP-3 levels have been reported to be significantly decreased after treatment with methotrexate or sulfasalazine or both together [29, 41–44]. These findings suggest that levels of MMP-3 are dependent on the type, duration and intensity of the pharmacotherapy. It is thus possible that differences in the therapeutic regimen between studies may explain some of the inconsistencies in the relation of MMP-3 to progression. Additional factors may include differences in disease duration and activity and variation in assay characteristics, which are not standardized between studies. Consistent with the results of a recent study [29], we confirmed that patient-reported functional assessments and clinical symptomatic indices were not useful in predicting radiological progression.

Inflammation markers, such as CRP and ESR, have been regarded as useful predictors of joint damage in RA. However, our study confirmed the recent findings of Young-Min [29], showing that when novel and more specific markers of joint tissue metabolism were included in the model, these unspecific laboratory tests were no longer predictive. Among these novel tissue turnover markers, the strongest and most consistent association with progression was observed for urinary CTX-II, a biochemical marker of cartilage degradation, a finding consistent with several previous studies involving patients with early RA receiving MTX or etanercept [19], very early RA receiving the COBRA combination therapy or sulfasalazine alone [45] or late RA treated with conventional DMARDs [29]. Taken together, the results from these previous studies and the current one suggest that urinary CTX-II is predictive of radiological progression across patient populations and independent of the type of therapy. We also found that urinary-Glc–Gal–PYD, a specific biochemical marker of synovial tissue metabolism, was associated significantly with radiographical progression in bivariate analysis. This result was consistent with that of a previous study [19] of early RA patients receiving methotrexate or etanercept. However, urinary-Glc–Gal–PYD did not remain in the final panel of predictors after multivariate analysis, confirming

the recent study of Young-Min [29] who showed that Glc–Gal–PYD was predictive in bivariate, but not in multivariate analyses when CTX-II was included in the model. This lack of independent predictive value is likely to be due to the high correlation of Glc–Gal–PYD with CTX-II ($r = 0.61, p < 0.001$) and suggests that in early active RA, degradation of cartilage is closely linked to synovitis. Whether urinary Glc–Gal–PYD could be an independent predictor of progression in late RA or in patients receiving biological therapies remains to be determined.

Previously published cross-sectional studies found an increased urinary PYD/DPD ratio in patients with RA [46–49]. Our study, however, is the first showing that U-PYD/DPD ratio is an independent predictor of radiological progression. Both PYD and DPD are non-reducible cross-links of mature collagen molecules, and they are believed to be important factors for maintaining the structure of the collagen fibril network in the matrix of the various tissues, including bone and cartilage. In healthy tissues, the PYD/DPD ratio is highest in cartilage (ratio: 50), intermediate in synovial tissue and tendons (ratio: 15–16) and lowest in bone (ratio: 3.5) [50–52]. The tissue PYD/DPD ratio can be altered in RA tissue, with the latter showing a higher ratio than healthy synovium [23, 51]. In addition, a high tissue PYD/DPD ratio in bone caused by the overhydroxylation of Lys at the helical cross-linking sites in type I collagen has been observed in the hip fracture cases [53] and osteoporosis [54]. Thus, the PYD/DPD ratio may theoretically provide some indication of the type of articular tissue that is predominantly degraded in RA. In our study, this ratio, but not PYD and DPD separately, was associated with radiological progression of bone erosion and JSN independently of CTX-II, which is a specific marker of cartilage degradation and of Glc–Gal–PYD (a specific marker of synovial metabolism), suggesting indeed the added value of this parameter. One possibility is that this ratio partially reflects structural alterations of bone tissue matrix associated with increased bone fragility, as suggested by some ex vivo biochemical studies [53, 54].

We found that high BMI was correlated negatively with the progression of joint erosion and JSN and that patients with lower values (<18.5), defined as underweight, had a 4.8-fold (95% CI 1.1–20) higher risk than the patients with higher BMI (>25) who were defined as overweight. Previously published reports showed a body weight loss due to disease activity [55–58] in RA, although no significant correlation between BMI and inflammation markers was observed at baseline in our study (data not shown). Our results agree with studies published previously by Kaufmann [23], Westhoff [31] and van der Helm-van Mil [30] which showed that high BMI was protective against the radiological progression in early RA. It has been suggested that the relationships between BMI and joint damage are mediated in part by the adipocytokines secreted by fat tissues. Interestingly, we recently reported that increased serum levels of adiponectin—which is negatively associated with BMI—are associated with a greater overall joint destruction in patients with RA [59]. Using a bivariate analysis, we found that triglycerides, but not total cholesterol and its subfractions were negatively correlated with radiological progression. However, in the multiple variable model, triglycerides were not an independent predictors, possibly because of its positive association with BMI ($r = 0.29, p < 0.001$).

Previously published data showed that high initial radiographical damage evaluated with TSS or the Larsen score was associated with subsequent radiological progression [16, 17] and that the initial erosion score in particular has a predicting value for radiological prognosis [14, 18, 23]. These data were analyzed without biochemical markers of joint tissue turnover as the initial factors; however, we found that baseline radiological joint damage of the extent of JSN was strongly and independently predictive of biochemical markers of joint tissue turnover associated with progression.

We believe that the four independent predictors of radiological progression we identified in this study may reflect different and complementary information of the various pathophysiological processes involved in joint destruction. The baseline Sharp score provides an estimation of the amount of joint destruction that has occurred, on average, during 2.3 years of disease duration before the start of the follow-up. Urinary CTX-II is a dynamic indicator of the rate at which cartilage tissue will deteriorate during the course of the disease. The PYD/DPD ratio may be related to increased bone fragility, and the BMI may provide integrated information on contribution of adipose tissue metabolism to maintain joint tissues health. These four independent predictors were statistically selected using those patients with high disease activity who were participating in the control arm of the SAMURAI study and who had >6 tender joints (of 49 evaluated), >6 swollen joints (of 46 evaluated joints), ESR of >30 mm/h and CRP of >2 mg/dl. These predictors may therefore be beneficial for targeting new biological therapies to patients with rapid progression of joint destruction.

Although our study covered one of the largest ranges of predictive variables for the progression of joint damage ever investigated concomitantly in the same population, due to sample volume limitation we could not analyze a number of the biochemical markers that have been reported to be associated with joint damage in RA, including anti-CCP antibody, cartilage oligomeric matrix protein (COMP) [25, 26, 60], osteoprotegerin (OPG) and Receptor Activator of Nuclear Factor-kappa B Ligand (RANKL) [61]. Our

study included patients with RA within 5 years of disease duration, so it remains to be determined whether the same set of predictive factors will also perform similarly in patients with earlier RA. Furthermore, our study could not clarify the prognostic factors in the each type of DMARDs treatment nor whether CTX-II, the PYD/DPD ratio, the JSN score and BMI predict progression independent of the type of DMARDs treatment, since the dose, type and combination of DMARDs and/or immunosuppressants was varied and changed according to disease activity at the discretion of the treating physician in our study. However, our data could provide the prognostic values of CTX-II, PYD/DPD ratio, JSN score and BMI in the actual clinical practice of RA treatment.

In summary, among of a panel of 40 different variables, we identified baseline joint damage, urinary CTX-II, the PYD/DPD ratio and BMI as strong and independent factors of radiological progression in patients with RA receiving conventional DMARDs. If confirmed in other studies, this set of few variables may be useful to identify patients with RA who are at high risk for disease progression.

Acknowledgments The authors wish to thank Takahiro Kakehi, B.Sc., Tamiko Kuraishi, B.Sc., Yukiyasu Mariko, M.Sc. and Yuichi Kawata, B.Sc., for their valuable assistance with the design and analysis of the study and preparation of this manuscript. This work was supported by Chugai Pharmaceutical Co., Ltd., Tokyo, Japan.

References

1. Kuper HH, van Leeuwen MA, van Riel PL, Prevoo ML, Houtman PM, Lolkema WF, et al. Radiographic damage in large joints in early rheumatoid arthritis: relationship with radiographic damage in hands and feet, disease activity, and physical disability. Br J Rheumatol. 1997;36:855–60.
2. Corbett M, Dalton S, Young A, Silman A, Shipley M. Factors predicting death, survival and functional outcome in a prospective study of early rheumatoid disease over fifteen years. Br J Rheumatol. 1993;32:717–23.
3. Drossaers-Bakker KW, de Buck M, van Zeben D, Zwinderman AH, Breedveld FC, Hazes JM. Long-term course and outcome of functional capacity in rheumatoid arthritis: the effect of disease activity and radiologic damage over time. Arthritis Rheum. 1999;42:1854–60.
4. Welsing PM, van Gestel AM, Swinkels HL, Kiemeney LA, van Riel PL. The relationship between disease activity, joint destruction, and functional capacity over the course of rheumatoid arthritis. Arthritis Rheum. 2001;44:2009–17.
5. Plant MJ, Jones PW, Saklatvala J, Ollier WE, Dawes PT. Patterns of radiological progression in early rheumatoid arthritis: results of an 8 year prospective study. J Rheumatol. 1998;25:417–26.
6. Fex E, Jonsson K, Johnson U, Eberhardt K. Development of radiographic damage during the first 5–6 yr of rheumatoid arthritis. A prospective follow-up study of a Swedish cohort. Br J Rheumatol. 1996;35:1106–15.
7. Fuchs HA, Kaye JJ, Callahan LF, Nance EP, Pincus T. Evidence of significant radiographic damage in rheumatoid arthritis within the first 2 years of disease. J Rheumatol. 1989;16:585–91.
8. van der Heijde DM. Joint erosions and patients with early rheumatoid arthritis. Br J Rheumatol. 1995;34:74–8.
9. Scott DL, Grindulis KA, Struthers GR, Coulton BL, Popert AJ, Bacon PA. Progression of radiological changes in rheumatoid arthritis. Ann Rheum Dis. 1984;43:8–17.
10. Gay S, Gay RE, Koopman WJ. Molecular and cellular mechanisms of joint destruction in rheumatoid arthritis: two cellular mechanisms explain joint destruction? Ann Rheum Dis. 1993;52:S39–47.
11. Ochi T, Iwase R, Yonemasu K, Matsukawa M, Yoneda M, Yukioka M, et al. Natural course of joint destruction and fluctuation of serum C1q levels in patients with rheumatoid arthritis. Arthritis Rheum. 1988;31:37–43.
12. Hulsmans HM, Jacobs JW, van der Heijde DM, van Albada-Kuipers GA, Schenk Y, Bijlsma JW. The course of radiologic damage during the first six years of rheumatoid arthritis. Arthritis Rheum. 2000;43:1927–40.
13. van der Heijde DM, van Riel PL, van Leeuwen MA, van 't Hof MA, van Rijswijk MH, van de Putte LB. Prognostic factors for radiographic damage and physical disability in early rheumatoid arthritis. A prospective follow-up study of 147 patients. Br J Rheumatol. 1992;31:519–25.
14. van Zeben D, Hazes JM, Zwinderman AH, Vandenbroucke JP, Breedveld FC. Factors predicting outcome of rheumatoid arthritis: results of a followup study. J Rheumatol. 1993;20:1288–96.
15. Mansson B, Carey D, Alini M, Ionescu M, Rosenberg LC, Poole AR, et al. Cartilage and bone metabolism in rheumatoid arthritis. Differences between rapid and slow progression of disease identified by serum markers of cartilage metabolism. J Clin Invest. 1995;95:1071–7.
16. van der Heide A, Remme CA, Hofman DM, Jacobs JW, Bijlsma JW. Prediction of progression of radiologic damage in newly diagnosed rheumatoid arthritis. Arthritis Rheum. 1995;38:1466–74.
17. Jansen LM, van der Horst-Bruinsma IE, van Schaardenburg D, Bezemer PD, Dijkmans BA. Predictors of radiographic joint damage in patients with early rheumatoid arthritis. Ann Rheum Dis. 2001;60:924–7.
18. Kaltenhauser S, Wagner U, Schuster E, Wassmuth R, Arnold S, Seidel W, et al. Immunogenetic markers and seropositivity predict radiological progression in early rheumatoid arthritis independent of disease activity. J Rheumatol. 2001;28:735–44.
19. Garnero P, Gineyts E, Christgau S, Finck B, Delmas PD. Association of baseline levels of urinary glucosyl-galactosyl-pyridinoline and type II collagen C-telopeptide with progression of joint destruction in patients with early rheumatoid arthritis. Arthritis Rheum. 2002;46:21–30.
20. Boers M, Kostense PJ, Verhoeven AC, van der Linden S. Inflammation and damage in an individual joint predict further damage in that joint in patients with early rheumatoid arthritis. Arthritis Rheum. 2001;44:2242–6.
21. Vittecoq O, Pouplin S, Krzanowska K, Jouen-Beades F, Menard JF, Gayet A, et al. Rheumatoid factor is the strongest predictor of radiological progression of rheumatoid arthritis in a three-year prospective study in community-recruited patients. Rheumatology (Oxford). 2003;42:939–46.
22. Green MJ, Gough AK, Devlin J, Smith J, Astin P, Taylor D, et al. Serum MMP-3 and MMP-1 and progression of joint damage in early rheumatoid arthritis. Rheumatology (Oxford). 2003;42:83–8.
23. Kaufmann J, Kielstein V, Kilian S, Stein G, Hein G. Relation between body mass index and radiological progression in patients with rheumatoid arthritis. J Rheumatol. 2003;30:2350–5.
24. Verstappen SM, Poole AR, Ionescu M, King LE, Abrahamowicz M, Hofman DM, et al. Radiographic joint damage in rheumatoid arthritis is associated with differences in cartilage turnover and